FCTUC FACULDADE DE CIÊNCIAS
E TECNOLOGIA
UNIVERSIDADE DE COIMBRA

Identification and Removal of Noise in Cardiac Signals (CARDIO-NOISE)

Diogo Barreiro Nunes

MASTER'S DEGREE IN BIOMEDICAL ENGINEERING

Physics Department

Faculty of Sciences and Technology of University of Coimbra

February 2016

Identification and Removal of Noise in Cardiac Signals (CARDIO-NOISE)

Author

Diogo B. Nunes

Supervisors

Professor Doutor César A. D. Teixeira

Professor Doutor Paulo F. P. de Carvalho

Dissertation presented to the Faculty of Sciences and Technology of the University of Coimbra to obtain a Master's degree in Biomedical Engineering

Coimbra, 2016

This thesis was developed in collaboration with:

Department of Computer Engineering

Center for Informatics and Systems of the University of Coimbra

WELCOME Project – Wearable Sensing and Smart Cloud Computing for Integrated Care to COPD Patients with Comorbidities

HeartSafe Project – Assessing Heart Function for Unsupervised Homecare Applications through Multi-Channel Auscultation

Esta tese é dedicada à minha mãe e ao meu irmão,

x

Acknowledgments

Gostaria de agradecer a várias pessoas pelo apoio, amizade e enriquecimento académico que dispus ao longo desta fase da minha vida. Sem elas, não teria sido o mesmo e eu não seria o mesmo.

Em primeiro lugar, agradeço ao Professor César Teixeira por ter fomentado em mim uma postura crítica e autocrítica, estando sempre disponível para trocar ideias e guiar-me da melhor forma. O mesmo se aplica ao Professor Paulo de Carvalho, que sempre se mostrou disponível para partilhar o seu conhecimento e experiência.

Não poderia deixar de agradecer também aos Professores Jorge Henriques e Rui Pedro Paiva pelas suas críticas construtivas e transmissão de conhecimentos ao longo da tese. Tal como ao Departamento de Engenharia Informática (DEI) que me acolheu, aos CISUC e aos projetos HeartSafe e WELCOME.

Por fim, agradeço aos amigos e familiares. À minha mãe e irmão que sempre me transmitiram a sua confiança. Ao Carlos, Luís, Diana e Samuel que fizeram do DEI uma segunda casa em Coimbra. Ao Jóni, André, Wilson, Joana, Carolina e Miguel pelo seu apoio e amizade. Ao Rafael, Fábio, Gonçalo e Mafalda e restantes amigos por estarem sempre presentes e fazerem de Coimbra uma experiência única. Finalmente, à minha colega e amiga Adriana, que foi um alicerce e grande fonte de motivação ao longo de toda a tese.

Abstract

The increase of population ageing and sedentary lifestyle of today's society leads to a greater demand for hospital services, which are unable to efficiently balance the demand with the supply [1]. This problem led to the development of automatic systems able to collect vital information from subjects on a daily basis, and through these, evaluate possible pathologies without the need for patients to request hospital services, thus, leading to a relief in demand and cost of medical consultations. These automatic systems are called tele-monitoring systems, which are integrated with biosensors to acquire bio-signals and computational algorithms to process them. These algorithms are mathematical methodologies which provide the necessary intelligence to the system in order to detect diseases and physiological information about a given subject. However, due to the ambulatory nature of such systems, the acquisition of bio-signals is exposed to numerous sources of noise, leading to the signals contamination. Noise can lead to wrong event algorithm behavior, therefore, in order to prevent pathological false detections it is essential to make the detection of contaminated periods. The focus of this thesis is noise detection in bio-signals, particularly in Phonocardiogram (PCG) and Electrocardiogram (ECG).

The noise detection methodology in the PCG context is characterized by being a real-time and multi-channel process. It can be divided into two phases: a first phase consists in searching a clean heart sound (HS) reference; the second phase compares this reference with the remaining test windows and evaluates the presence of noise based on the spectral similarity and the ratio of the total amount of high frequency components, between the reference and test windows. In healthy signals the algorithm achieved a sensitivity and specificity of 91.24% and 90.88%, respectively. In pathological signals it reached a specificity of 91.68%. Its computational cost is 0.17s per minute of PCG signal at 4000Hz. It was also compared on the same testing dataset with the methodologies that presented the highest precision rates in literature, namely the Modulation Filtering algorithm [2] and the Periodicity Based algorithm [3]. Additionally to the better results presented by our algorithm, it was also more computationally efficient than the compared methodologies.

The ECG noise detection methodology uses the Principal Component Analysis (PCA) approximation error of each heartbeat and the presence of high frequency components to evaluate the presence of noise in 4s periods in signals lasting at least 5 minutes. In the testing dataset it achieved 94.08% and 89.88% of sensitivity and specificity, respectively, at critical SNR levels. Its computational cost is 0.14s per 5 minutes of ECG sampled at 250 Hz. The highest documented precision in literature is 96.63% and 94.74% of sensitivity and specificity, respectively, using an algorithm based on Empirical Mode Decomposition (EMD) [4]. However, the authors only considered noise corruption in the cases where the R-peaks were not recognizable, suggesting that the presented precision is only valid for high degrees of noise. Additionally, our algorithm takes less time to compute five minutes of ECG than the EMD algorithm takes to compute five seconds.

Given the results, we believe that the developed methodologies fulfil the proposed goals with high precision levels and low computational costs. It would be interesting to see how the algorithms behave in real situations and uncontrolled environments in order to assess its real use in tele-monitoring systems.

Resumo

O envelhecimento da população e o estilo de vida sedentário da sociedade atual resulta numa maior procura de serviços hospitalares, serviços esses incapazes de balancear eficazmente a procura com a oferta [1]. Este problema levou a desenvolver sistemas automáticos capazes de recolher informações vitais no dia-a-dia dos pacientes, e através destas avaliar possíveis patologias, sem que os pacientes se deslocassem aos serviços hospitalares, levando assim a um alívio na procura e custo de consultas médicas. Estes sistemas automáticos são denominados de sistemas de tele-monitorização, onde algoritmos computacionais são integrados em sistemas compostos por biossensores. Estes algoritmos são metodologias matemáticas que dão ao sistema a inteligência necessária para conseguir detetar patologias e informações fisiológicas sobre um determinado sujeito. Porém, devido à natureza ambulatória destes sistemas, a aquisição de bio sinais está sujeita a inúmeras fontes de ruído, levando à contaminação dos sinais. A distorção dos sinais devido ao ruído pode levar os algoritmos de deteção de patologias a detetar características patológicas quando elas não estão presentes, ou vice-versa. Por isso é imprescindível que se faça a deteção dos períodos que estão contaminados, de forma a não resultar em falsas deteções patológicas. Esta tese foca-se no âmbito da deteção de ruído em bio sinais, nomeadamente, em Fonocardiograma (PCG) e Eletrocardiograma (ECG).

A metodologia de deteção de ruído em PCG caracteriza-se por ser em tempo real e multicanal. Pode ser dividida em 2 fases: uma primeira onde se procura uma referência limpa de som cardíaco (HS); e uma segunda onde se compara essa referência com as restantes janelas de teste e se avalia a presença de ruído com base na semelhança espectral e a razão da soma dos componentes de altas frequências entre a referência e as janelas de teste. A metodologia atingiu uma sensibilidade e especificidade de 91.24% e 90.88%, respetivamente, em sinais saudáveis. Em sinais patológicos atingiu uma especificidade de 91.68%. O seu custo computacional é de 0.17s por minuto de sinal PCG a 4000Hz. A nossa abordagem foi também comparada com as metodologias que apresentam a maior precisão na literatura, nomeadamente o algoritmo Modulation Filtering [2] e o algoritmo Periodicity Based [3]. Para além de melhores resultados, a nossa metodologia também apresentou uma maior eficiência computacional.

A metodologia de deteção de ruído em ECG utiliza o erro de aproximação por Principal Component Analysis (PCA) de cada batimento cardíaco e a presença de componentes de altas frequências para avaliar a presença de ruído em períodos de 4s em sinais com duração de pelo menos 5 minutos. No dataset de teste atingiu 94.08% e 89.88% de sensibilidade e especificidade, respetivamente. O seu custo computacional é de 0.14s por 5 minutos de ECG a 250 Hz. A maior precisão documentada na literatura é de 96.63% e 94.74% de sensibilidade e especificidade, respetivamente, recorrendo a um algoritmo baseado na Empirical Mode Decomposition (EMD) [4]. Porém, os autores apenas consideram contaminação por ruído nos casos onde os picos R não são reconhecíveis, sugerindo que a precisão documentada é apenas válida para altos níveis de ruído. Para além disso, o nosso algoritmo leva menos tempo a processar 5 minutos de ECG do que o algoritmo baseado em EMD leva a processar 5 segundos.

Dados os resultados, consideramos que as metodologias desenvolvidas cumprem os objetivos, com altos valores de precisão e baixos custos computacionais. Seria interessante ver como os algoritmos se comportam em situação real e em ambiente sem controlo para poder avaliar o seu verdadeiro uso em sistemas de tele-monitorização.

List of Publications

D. Nunes, A. Leal, R. Couceiro, J. Henriques, L. Mendes, P. Carvalho, C. Teixeira, "A low-complex multi-channel methodology for noise detection in phonocardiogram signals," in *Engineering in Medicine and Biology Society (EMBC), 2015 37th Annual International Conference of the IEEE* , vol., no., pp.5936-5939, 25-29 Aug. 2015 doi: 10.1109/EMBC.2015.7319743.

P. Carvalho, J. Henriques, C. Teixeira, R. Couceiro, T. Rocha, L. Mendes, **D. Nunes**, I. Chouvarda, N. Maglaveras, R. Paiva, "Biodata Analytics for COPD," submitted in: *3rd International Conference on Biomedical and Heath Informatics (BHI), 24-27 February 2016*.

List of Figures

List of Tables

Contents

Chapter 1 – Motivation and Objectives

Cardiovascular diseases are the main cause of decease in Europe, being responsible for 46% of the total mortality [5] and is estimated that costs €196 billion per year to the EU economy [6]. Due to the increasingly population ageing, these costs are predicted to grow, if no new strategies are adopted.

One of the strategies used to control the high demand of hospital services and decrease the overall costs is the consideration of Telemedicine systems [7], where the main objective is to move from a system centered in the Hospital to a system centered on the Patient. Therefore, quality service is offered at a lower cost, where the access to the specialized services is decentralized and the investment is made on a preventive clinic rather than a curative clinic, with a higher participation from the patient.

The work developed in this thesis is in the context of one of the Telemedicine areas, the Tele monitoring, where devices, like vests or beds with integrated sensors are used to acquire bio-signals (e.g. electrocardiogram (ECG), phonocardiogram (PCG) or Respiratory Lung Sounds (RLS)). Computational algorithms are then used to process and analyze various physiological features and/or pathologies [8]. These apparatus are also known as Personal Telehealth Systems, or just pHealth systems. However, due to the ambulatory nature of such signal acquisition, it is expected that noise sources will affect signals, changing the original information. The presence of noise artifacts is a serious problem when the assessment of some pathologies is performed, since it may distort the signal in a way that either hides, or mimics pathologic characteristics, leading to misdiagnosis [9]. Therefore, a methodology that differentiates the signal from noise artifacts is required, to prevent erroneous decisions when it comes to diagnosis.

The purpose of this work is therefore to develop noise detection algorithms for the PCG and ECG signals. The particular choice of PCG and ECG signals is based on the high mortality rate caused by cardiovascular diseases, thus so, being natural candidates to integrate in tele monitoring systems. A low computational cost is sought in order to make the algorithms feasible to be integrated in pHealth systems. The noise-contaminated periods identified by the algorithms are then excluded from further analysis, thus avoiding misdetection of pathologies. A noise detection strategy was chosen in favor of a noise reduction/reconstruction one because there is a great amount of available signal in the tele-monitoring context. Additionally, the noise reduction approach may distort the original signal due to the filtering processes, hiding some important features for diagnosis.

Chapter 2 – Background Concepts and State of the Art

2.1 Cardiac anatomy and physiology

The heart is responsible for pumping the blood through the entire body, generating the driving force required for this vital task. It is divided in two sections, left and right, separated by the septum, each side composed by an atrium and a ventricle (see **Figure 2.1**). The right atrium receives the deoxygenated blood from the body and pumps it to the right ventricle, which in turn pumps it to the lungs for oxygenation. The arterial blood enters in the left atrium by the pulmonary veins, which passes it to the left ventricle, which in turn pumps it to the entire body again. The atrioventricular valves separate the atria and ventricles, namely the tricuspid valve on the right side and the mitral valve on the left side. There is also the pulmonary valve that separates the right ventricle and the pulmonary artery, and the aortic valve, that borders between the left ventricle and aortic artery, collectively known as semilunar valves.

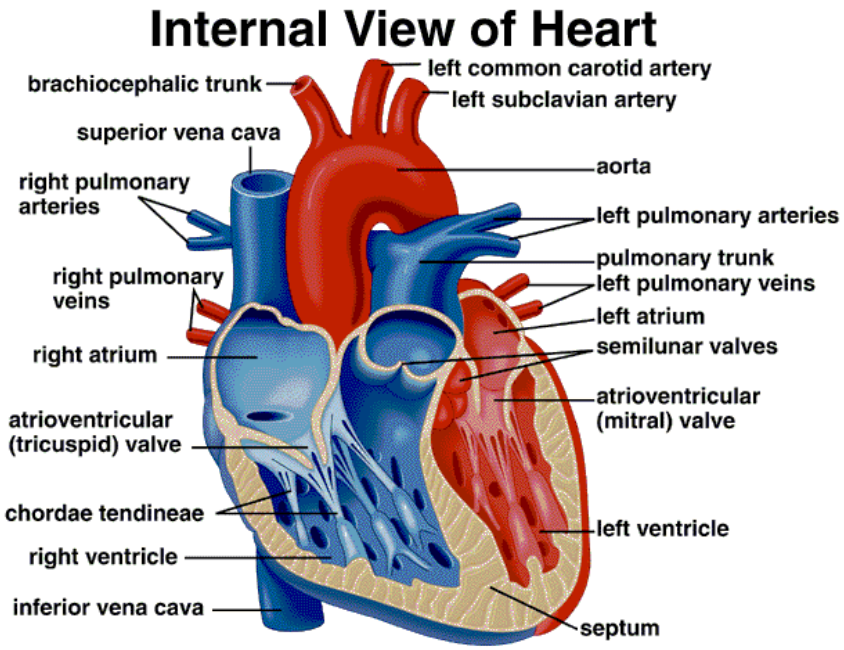

Figure 2.1 – *Basic anatomy of the heart (extracted from* [10]*).*

The valves are responsible for directing the blood flow, not allowing an inversion in blood circulation. The valves are formed by strong fibrous cords, named *chordae tendineae*, which are connected to the cardiac epithelium. Depending on the pressure profile existing on the different chambers, the valves will or will not allow the blood flow.

The driving force is generated due the chambers contraction, which is regulated by electrical impulses sent by the autonomous nervous system to the heart. The electrical activity of the heart results in action potentials conducted by a specialized nervous tissue and the cardiac muscle. The Electrocardiogram (ECG) measures the heart electrical activity. A normal heartbeat is initiated in the sinoatrial (SA) node, which receives an electrical stimulus from the autonomous nervous system to start a new cardiac cycle. This stimulus is forwarded to the atrial muscle, which results in a depolarization wave through the walls resulting in an atrial contraction, and to the atrioventricular (AV) node. The AV node is the only transmission pathway from the SA node to the ventricles in a healthy heart (see **Figure 2.2**). The only purpose of this AV node is to delay the impulse conduction to the ventricles, giving enough time to the atria to complete its contraction. After the atrial contraction, the electrical impulse is conducted through the septum by the *bundle of His* which branches in *right bundle branch* and *left bundle branch* ending in the *Purkinje* fibers, which are responsible for the transmission of the electrical impulse to the ventricular muscle. When the ventricular muscle is stimulated, the depolarization wave travels from the endocardium to the epicardium, resulting in a ventricular contraction and in the consequent blood ejection to the arteries.

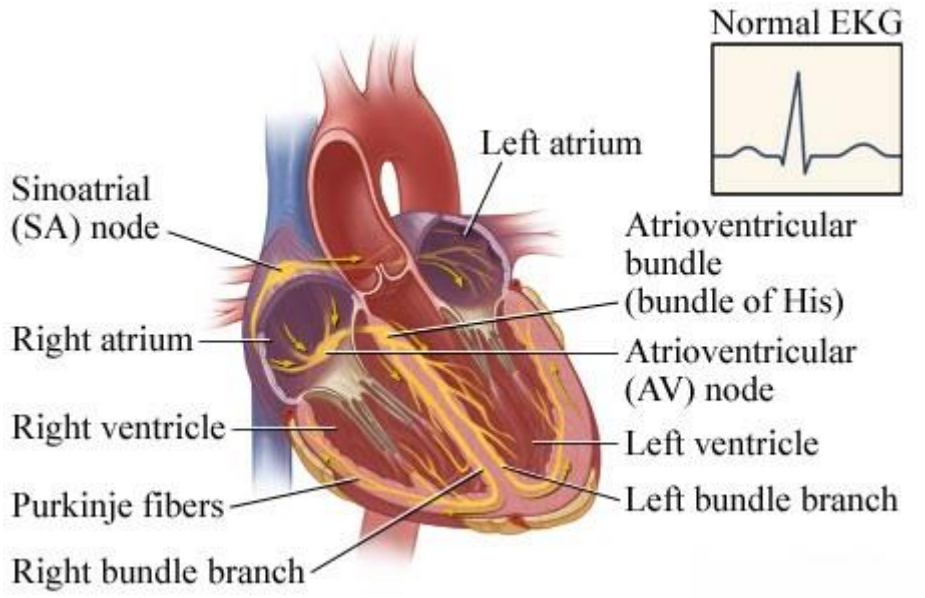

Figure 2.2 – *Cardiac nervous tissue (extracted from http://saintlukeshealthsystem.org).*

2.2 The cardiac cycle and origin of the heart sounds (HS)

The heart cycle is regulated by the electrical activity of the heart, regulating the contraction of the atria and ventricles. It comprises two phases, systole and diastole. Systole begins with the ventricular contraction, which increases the pressure inside the ventricular lumen. Rapidly, the pressure inside the ventricles exceeds the atrial pressure, resulting in the closure of the AV valves, originating the first heart sounds (HS), named S1. After the closure of the AV valves, an isovolumetric contraction happens until the ventricular pressure exceeds the pressure existing on the output arteries of the heart. When the ventricular pressure is superior to the arteries pressure, the semilunar valves open resulting in the blood ejection into the pulmonary and aortic arteries. The systole ends when the pressure of the output arteries exceeds the ventricular pressure, resulting in the closure of the semilunar valves and giving rise to the second HS, known as S2. The closure of the valves ends the blood ejection into the arteries.

After the closure of the semilunar valves an isovolumetric relaxation occurs, lowering the ventricular pressure. When the pressure inside the ventricles is lower than in the atria, the AV valves open, allowing the entrance of blood to the ventricular lumen. After that, an atria contraction happens, named atrial systole, which causes the remaining blood present in the atria to enter into the ventricles. This phase of ventricular

relaxation and filling, is named diastole. The process is repeated with the beginning of a new systole.

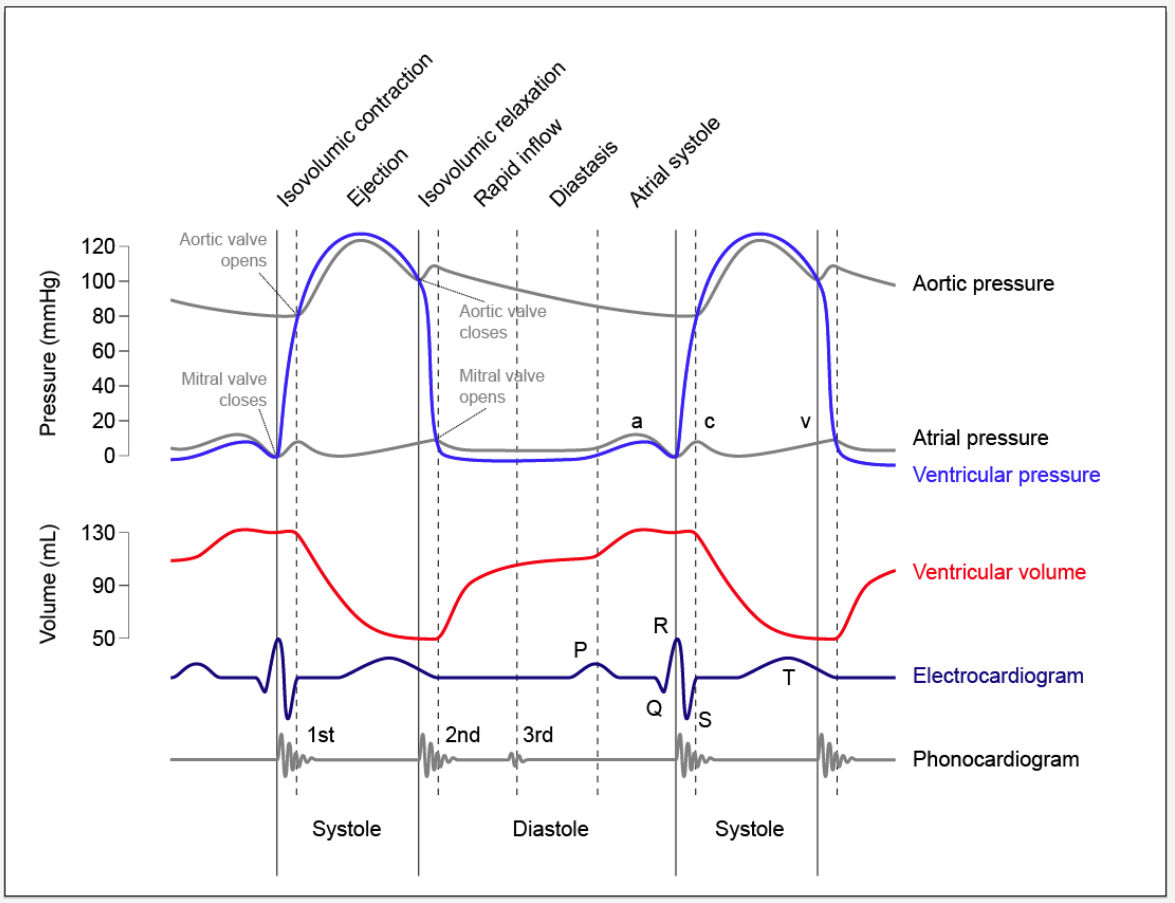

Figure 2.3 – *Main events in the cardiac cycle, and corresponding volume and pressure profiles (extracted from* [11]*).*

2.2.1 Phonocardiogram (PCG)

The phonocardiogram is a graphical representation of the HSs. This plot of the sound waves allows the investigation of a wider extent of features than the auscultation itself, thus being a highly efficient tool for diagnosis of some cardiac pathologies [12]. The phonocardiogram is recorded using microphones, which can be later represented and processed. In **Figure 2.4** is shown an example of a PCG segment in the temporal and frequency domain.

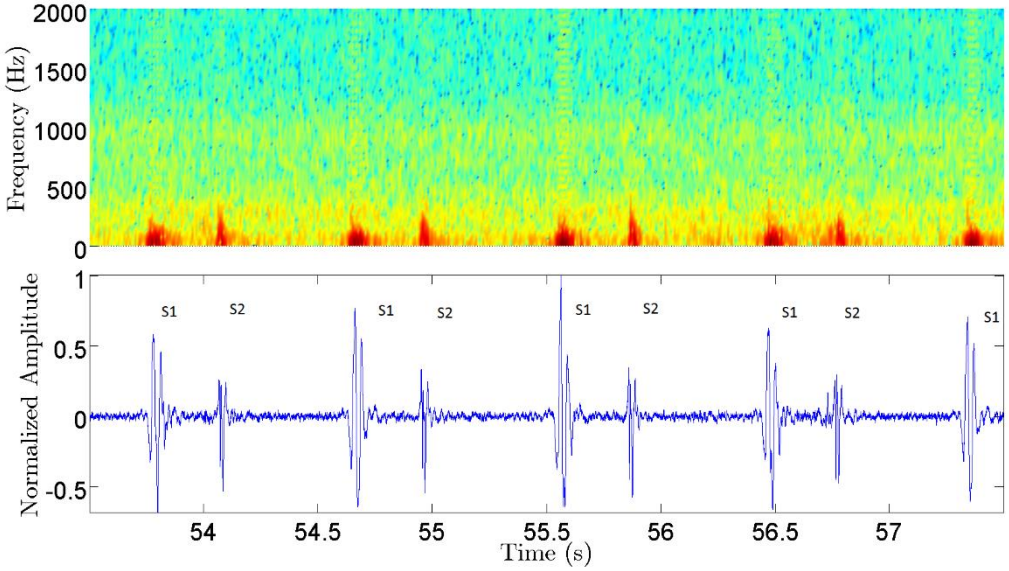

Figure 2.4 – *Typical sound wave and spectrogram of a PCG signal.*

2.2.2 *Heart sound physiology*

The HSs existing in the cardiac cycle are originated by the closure of the valves, blood flow and vibrations of the heart muscle. Typically, there are four HSs in a cardiac cycle. The first, S1, is clearly audible in the apical zone and in the fourth intercostal space in the left side of the sternum. It is characterized by a large amplitude and time duration when compared to the remaining HSs, having an average duration of 100-200ms. Observing the spectral distributions of S1, it is possible to identify two prominent frequency components in the 10-200Hz range. Although it is not consensual, the evidence points that these two frequency components are due to the mitral and tricuspid valve closure [11]. The properties of S1 are of great importance in the assessment of cardiac pathologies. They reflect the functioning of the AV valves and the force of the myocardium contraction. Another important characteristic of this HS is the temporal delay between the closure of the tricuspid and mitral valve, which lasts in average 20-30ms in a normal heart. If this time delay is much higher than normal, then is a strong indicator of heart disease [11].

The second HS (S2) occurs in the beginning of diastole, and corresponds to the closure of the semilunar valves. It is audible in the second and third intercostal space on the left side of the sternum, and presents two main frequency components, which are associated with the aortic and pulmonary arteries closure. Higher frequency

components can be identified in the S2 spectrum, when comparing to S1. The second HS also presents a temporal delay between the closures of the two semilunar valves, but in this case, this delay is of greater duration. This is due to a higher pressure in the aortic artery comparing to the existing one in the pulmonary artery, causing the aortic valve to close before the pulmonary valve. The closing of the aortic and pulmonary valves are two events typically heard during auscultation. The time delay between these two events varies depending on the respiratory movements. In expiration, the duration of the delay is less than 30ms, whereas in inspiration this delay is of greater duration being clearly noticeable. The amplitude of the two components of S2 and the duration of the delay between them, are valuable information for cardiac disease diagnosis [13].

The third HS (S3) is usually referred as gallop sound, such as the fourth HS (S4). Both are low intensity and low frequency sounds, normally not audible in adults and occur in the beginning and end of diastole, respectively. S3 has its origin in the vibrations of the ventricular walls caused by the rapid inflow of blood into the ventricles. Its audition is a sign of pathology, but is natural in children and young adults. In patients with mitral regurgitation, the S3 is normally audible but don't imply necessarily systolic dysfunction or high ventricular pressure. In patients with aortic stenosis, S3 is less frequent [11].

S4 is caused by the ventricular walls distension when atria contraction happens. Normally is not noticeable, but when it is, it is sign of reduced distensibility in one or the two ventricles. The low ventricular distensibility causes the ventricular walls to make abrupt movements when the atria contraction occurs, originating vibrations, which produces the S4.

Certain HSs or heart features may be more perceptive in some areas of the chest, therefore there are multiple auscultation sites, which are depicted in **Figure 2.5**.

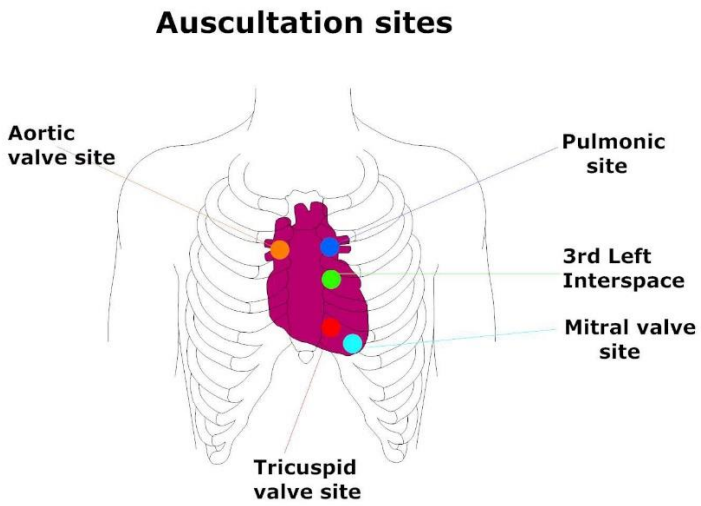

Figure 2.5 – *Auscultation sites (extracted from* [11]*).*

2.2.3 Pathological sounds

There are two main types of pathologies associated with valvular diseases and detected in cardiac auscultation: the cardiac stenosis and cardiac insufficiency. The stenosis is characterized by damage in the heart valves: where these valves lack the ability to fully open. The blood is thereby forced to pass through the small opening at a higher speed, causing a turbulent regime, and producing a sound. The valvular insufficiency or regurgitation is characterized by the back flow of the blood, due to the incomplete closure of the valves. Depending on the location of the heart valve deficiency, the stenosis or insufficiency may be mitral, tricuspid, pulmonary or aortic.

The sounds associated with pathologies are called cardiac murmurs and are originated by vibrations caused by turbulent blood flow in the cardiac structure. They are normally noticeable in children and after physical exercise, without being correlated with disease [11]. However, except for those cases, their presence may indicate stenosis or insufficiency in the aortic, pulmonary or mitral valves. Information about the occurring time and site they occur have great diagnosis value in cardiac diseases [11]. In addition to the cardiac murmurs, the S3 and S4 may also be associated with pathologies as mentioned before.

Finally, innocent murmurs can also be heard not being however associated with disease. Usually, they are cause by a high cardiac debit or by the reduction of the blood viscosity.

2.2.4 Noise sources in PCG

Noise sources affecting PCG may have an external or internal origin. External noise, or ambient, comprises any sounds which are produced in the environment where the acquisition takes place, such as music, people talking in the background, a door closing, and so on. The noise with an internal origin is all the noise produced inside the subject's body, such as speech, deep breathing, laughing and others. Typically, noise artifacts are characterized by the presence of higher frequency components in the spectrum than the existing ones in the clean PCG spectrum (see **Figure 2.6**, **Figure 2.7** and **Figure 2.8**).

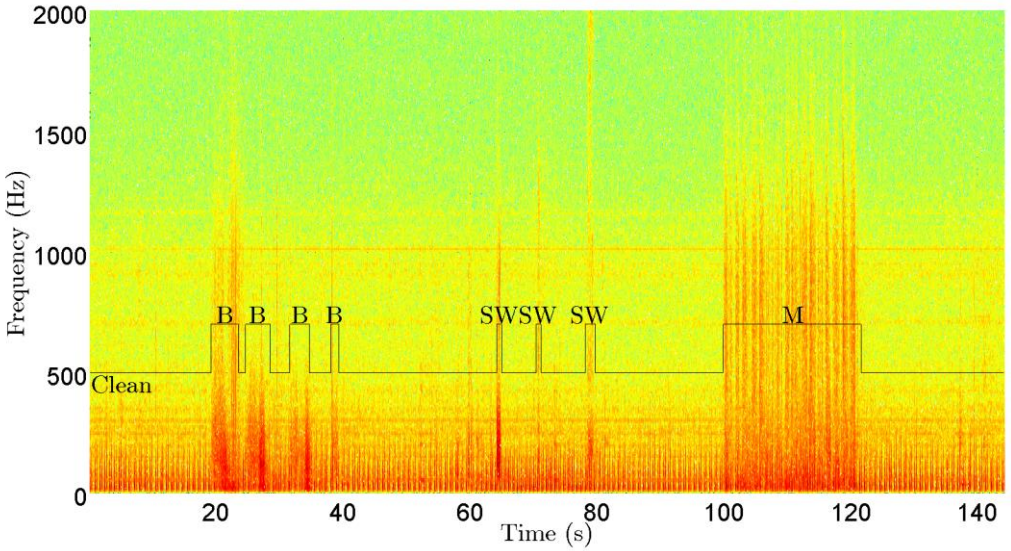

Figure 2.6 – *Spectrogram of a PCG signal contaminated by periods of physiological noise. 'B', 'SW' and 'M' corresponds to the artefacts originated by deep breathing, swallowing and body movement, respectively.*

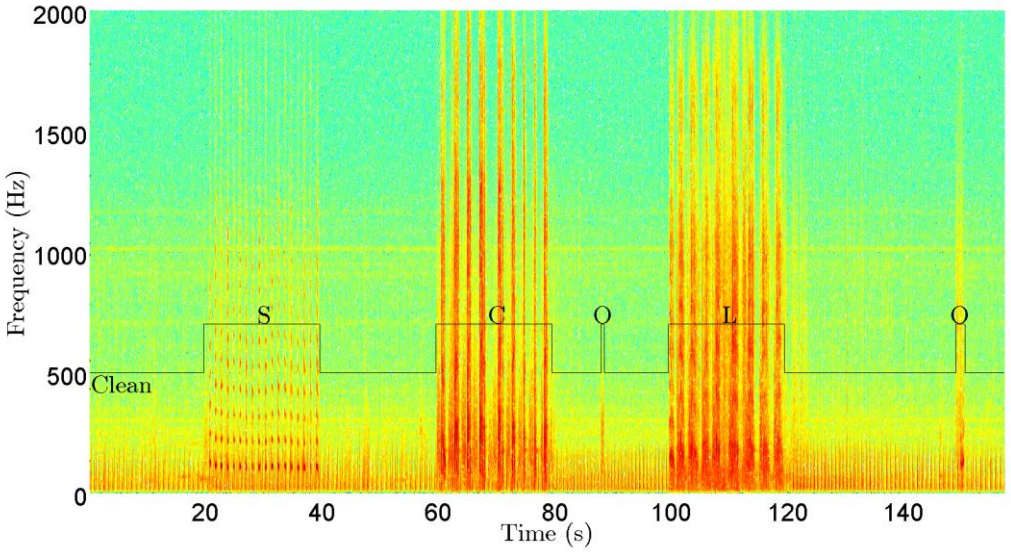

Figure 2.7 – *Spectrogram of a PCG signal contaminated by periods of vocal noise. 'S', 'C' and 'L' and 'O' corresponds to the artefacts originated by speech, cough, laugh and other types, respectively.*

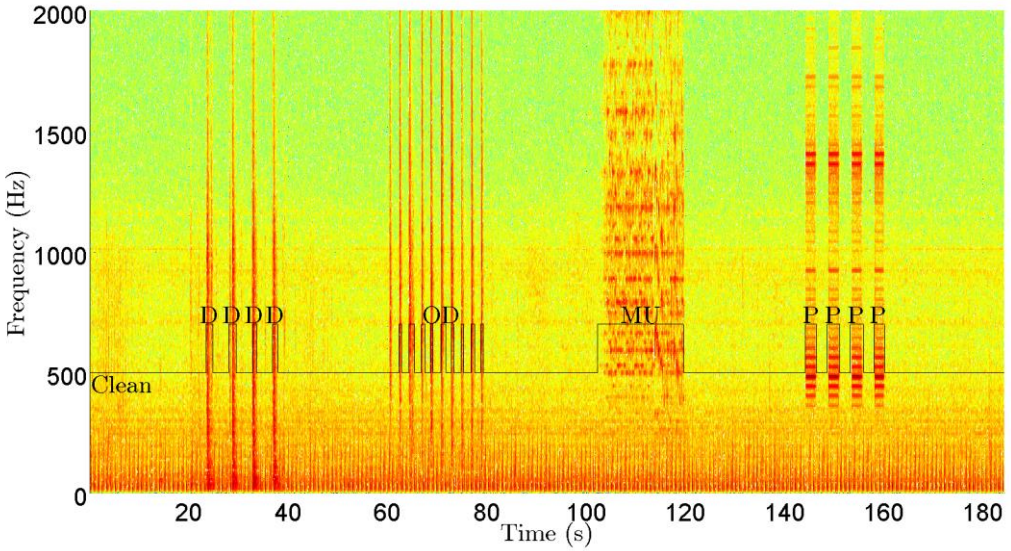

Figure 2.8 – *Spectrogram of a PCG signal contaminated by periods of ambient noise. 'D', 'OD' and 'MU' and 'P' corresponds to the artefacts originated by door closing, object drop, music and phone ringing, respectively.*

2.2.5 Noise treatment in PCG

Some strategies were already proposed to detect noise-contaminated periods in PCG signals.

In [2], a framing of the signal is performed in three seconds windows, followed by an evaluation of the stationarity in each window. This algorithm assumes the presence of two components in PCG signals: a stationary and periodic component related with respiratory sounds; and the quasi-stationary component related to HSs. The main goal of the algorithm is the detection of interferences in the stationary component of the signal, caused by transient noise sources. This is done by computing the short-time Fourier transform (STFT), followed by filtering the temporal trajectories of each frequency bin using a low-pass linear phase filter with a cut-off frequency of 1Hz, this operation is coined as modulation filtering. Then, power ratios of differently sized sub windows are extracted from the filtered temporal trajectories of each 3 second window. Finally, classification of noise is done using a Support Vector Machine (SVM) classifier.

In [3] a bi-phase algorithm is presented. The first phase consist in the search for a clean HS window that will be used as a template. In the second phase the found template window will be compared with the remaining windows. The selection of the reference window is based on periodicity signatures within a 4s window. The second phase compares the spectral similarity and the maximum energy ratio between the reference window and the remaining test windows to assess about the noise contamination in the HS clips.

In [14] noisy periods are detected by feeding single layer perceptrons, which were previously trained with clean and noisy data, with the wavelet coefficients of half second windows of PCG. In another study [15], different heart cycles are segmented resorting to an ECG gating. Afterwards, the mean correlation of the Spectral Power Distributions of the different cycles is obtained in order to ascertain about the presence of noise in a given PCG containing 10 heart.

In [16] is also presented a methodology that uses the ECG gating to segment the different heart cycles, but in this case, each heart cycle is divided in systole and diastole. Each systole period is divided in two different segments the variance of each one is computed. If the variance of one segment is superior to a given threshold, then, that segment is classified as contaminated. Next, the systoles are divided in more segments and if the standard deviation of each segment is lower than a given threshold, then that

segments is considered noise free. Finally, the correlations between the systoles are computed, and the ones with a higher correlation than 0.7 are considered noise free. The same methodology is used in the diastole segments.

In addition to the above described methodologies in noise detection periods to be posteriorly discarded, other noise reduction/cancelation methods have been developed, namely in [17][18][19].

In [17] a speech enhancement method, based on the spectral domain minimum-mean squared error (MMSE) estimation, is used to infer about presence of noise. In [18] an extra microphone is used to record only interferences produced by external noise sources, in order to perform noise subtraction to the signal containing the HSs. In [19] the PCG is filtered in a defined band frequency in order to enhance the HS and reduce the noise influence in the signal.

2.3 The cardiac cycle and the electrocardiogram (ECG)

The ECG consists in the recording of the action potentials in the heart. The depolarization and repolarization waves are measured using a galvanometer, which is an instrument that measures current. The type of wave, direction and intensity, determines the ECG profile. A depolarization wave approaching the positive electrode will produce a positive voltage, while moving away produces a negative voltage. The registered amplitude is directly proportional to the muscle mass where the wave was produced. For this reason, the waves originated in the ventricles present a higher amplitude due to its higher muscle mass. Depending on the sensors location, it is possible to obtain different perspectives from heart electrical activity. The different sensors configurations are known as leads.

2.3.1 ECG origin

Usually, there are four main waves registered in an ECG, each from a different cardiac occurrence:

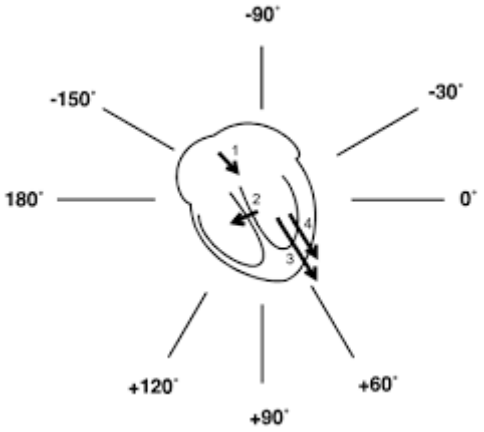

1. Depolarization wave corresponding to the atrial contraction.
2. Depolarization wave from the septum.
3. Depolarization wave from the ventricular muscle tissue.
4. Repolarization wave from the ventricular muscle tissue.

Figure 2.9 – *Polarization waves of the cardiac events (extracted from* [20]*).*

The depolarization waves do not travel in a straight line like depicted in **Figure 2.9**, instead they spread in all possible directions from the source point. However, the vector sum of the wave results in a unique vector with the average direction and intensity, named force vector. In **Figure 2.9** it is depicted the frontal plane of the heart, where the angles represent the different electrical axis for action potential measure. In this plane, six different perspectives, or leads, are used to measurement: the standard limb leads (I, II, e III, with the electrical axis situated in 0°, 60°, and 120°, respectively) and the augmented limb leads (aVR, aVL, and aVF, with the electrical axis situated in -150°, -30°, and 90°, respectively), in their whole named limb leads. These six leads can also be represented in the Einthoven triangle depicted in **Figure 2.10**.

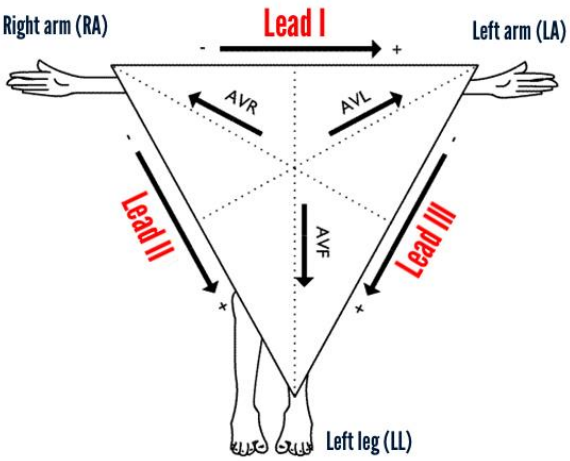

Figure 2.10 – *Einthoven triangle (extracted from* [21]*).*

In the atrial depolarization the force vector has an electrical axis close to the 60°, where the lead II axis is situated, so it is expected a positive voltage in the lead II, at this positive deflection is called P wave. In lead III this deflection is almost unnoticeable because the axis of this lead is almost perpendicular to the wave direction.

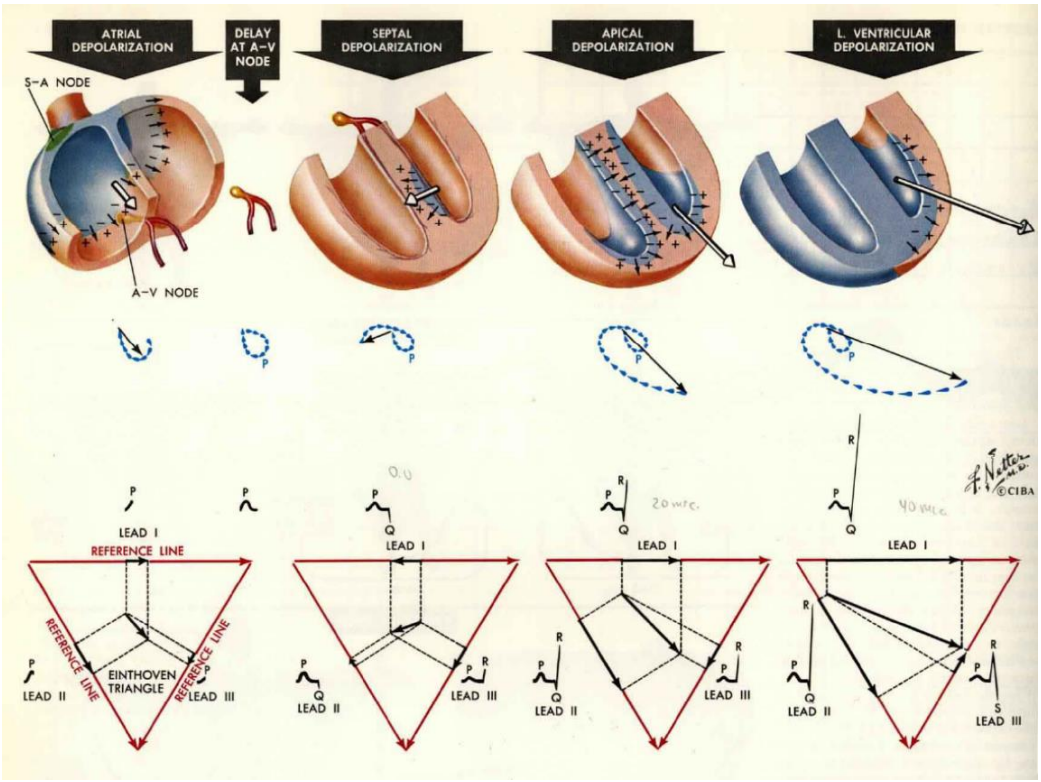

Figure 2.11 – *ECG formation, Part I (extracted from* [22]*).*

The next depolarization wave is the one that occurs from the septum, with its electrical axis near the 150°. As this wave is nearly perpendicular to the lead II axis, its

influence in the respective ECG is diminished, presenting a small negative deflection, since the projection of the force vector in the lead II axis is in the opposite way. In lead I the influence of this depolarization is more noticeable, since the wave and lead direction are close to each other, but of opposite ways, which reflects in a negative deflection. To this negative deflection caused by the septum depolarization is given the name of Q wave.

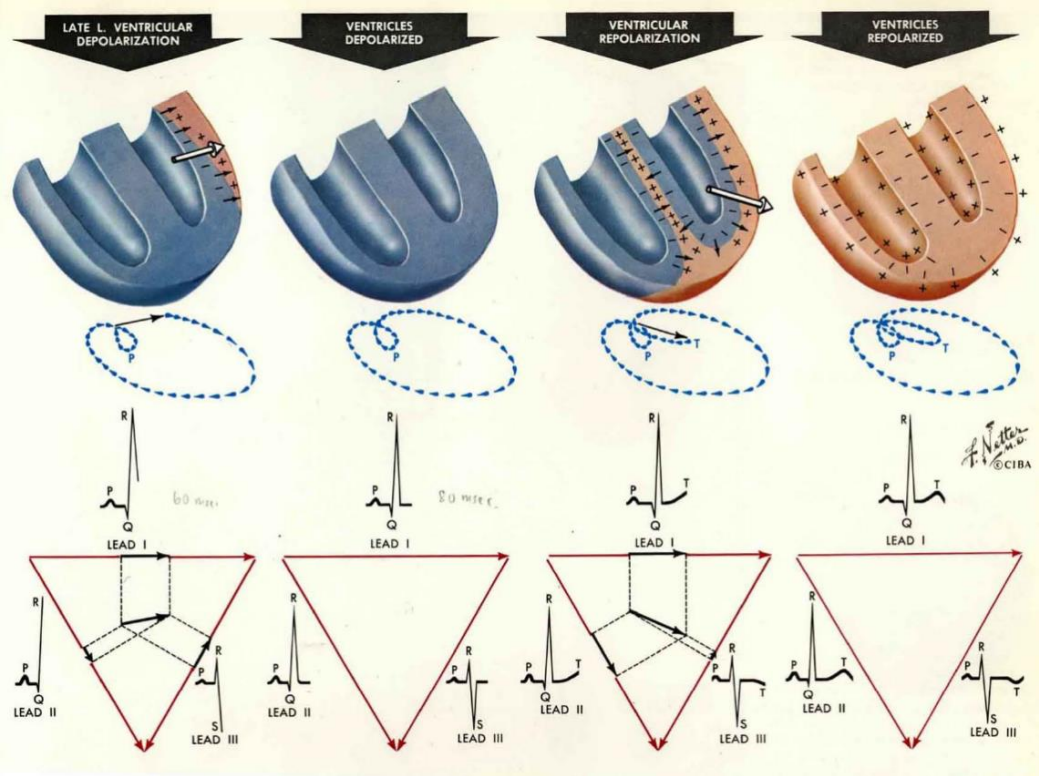

Figure 2.12 – *ECG formation, Part2 (extracted from* [22]*).*

Next, the depolarization wave travels through the apical zone with an axis close to 60°, reflecting a positive deflection in the three standard limb leads called R wave. The depolarization continues from the endocardium of the left ventricle to the epicardium. Since the wave projection in the late stage of ventricular depolarization is contrary to the lead III axis, there will be a negative deflection in voltage known as S wave. In the end of the heart cycle occurs the ventricular repolarization, causing the T wave.

In addition to the limb leads, there are more 6 leads which 'look' at the heart in the transverse or horizontal plane in different perspectives, called V leads, presented in **Figure 2.13**. The respective representations in the ECG depend on the electrical axis

of each wave and on lead in the horizontal plane. The same principles of ECG formation in the limb leads apply to the V leads.

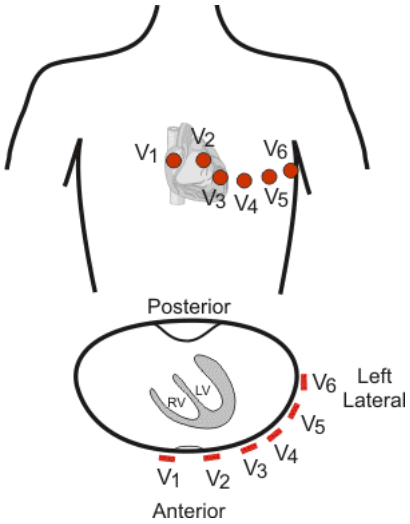

Figure 2.13 – *The unipolar chest leads, or V leads (extracted from* http://*cvphysiology.com).*

A normal 12-lead ECG presents the following form.

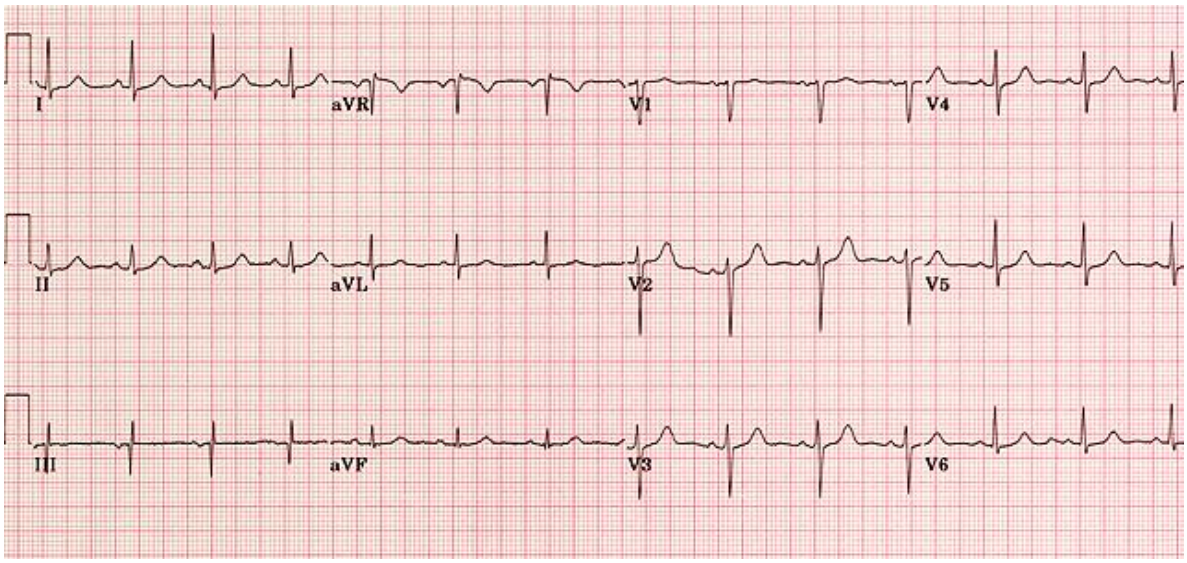

Figure 2.14 – *A normal 12-lead ECG (extracted from* http: // *pathology.wum.edu.pl).*

2.3.2 *Typical ECG of one heart cycle*

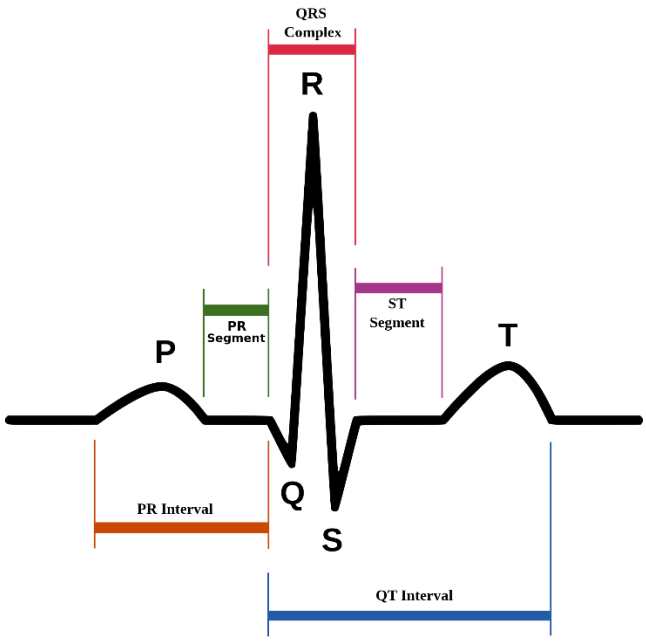

Figure 2.15 – *The QRS Complex (extracted from* http://*studyblue.com).*

- **P Wave:** Wave resulted from the atrial depolarization. Its absence may indicate a cardiac anomaly such as atrial fibrillation, while abnormally large amplitude may indicate a greater amount of atrial muscle than normal [20].
- **QRS Complex:** Complex formed by the Q, R and S waves. As it is the result of the ventricular depolarization, a greater mass is involved, resulting in a greater amplitude. Abnormalities in this complex may indicate severe anomalies [20].
- **T Wave:** Wave resulted from the ventricular repolarization. Inversion of the T wave with respect to the QRS complex and abnormal variations in amplitude, frequency and symmetry of the waveform in some leads are considered indicators of certain pathologies [20].

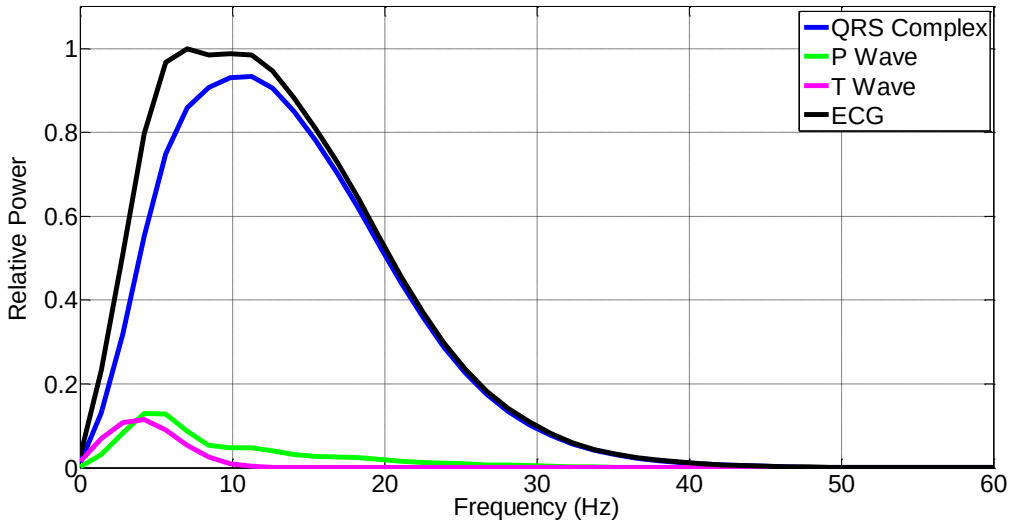

Figure 2.16 – *Spectral distribution of the different ECG waves.*

2.3.3 Noise sources in ECG

There are three main noise sources in an ECG (see **Figure 2.17**):

- Electrode Motion (EM).
- Muscle Artifact (MA).
- Baseline Wondering (BW).

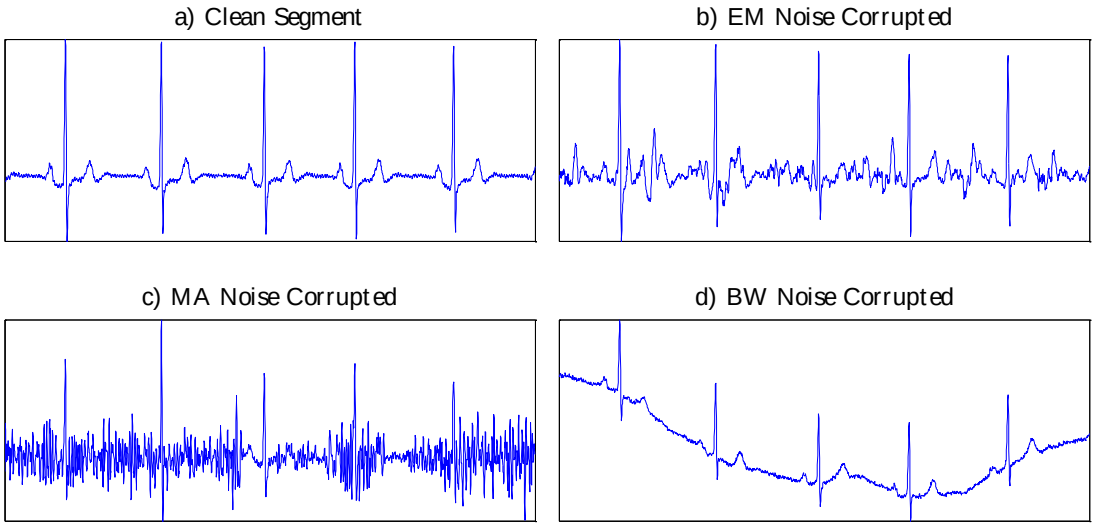

Figure 2.17 – *The main noise types influence on the same ECG segment.*

The EM noise is originated from the movement of the electrodes attached on the body and is caused by body position changes, that leads to electrode-skin impedance variations. This type of noise is considered the most troublesome since its frequency spectrum overlaps with the spectrum of the QRS. Its presence may mimic some ectopic beats and is difficult to be removed comparing to the other noise types [23],[24].

Muscle noise (MA) is caused by action potentials created by the muscles surrounding the heart, with overlapping frequency components with the ECG signal. This noise has also frequency components superior to the ones found in the clean ECG [23],[24],[25].

The BW noise is characterized by oscillations of the ECG baseline, which are usually caused by chest movements produced during breathing. It is characterized by low frequencies, in the range of 0.1-1Hz [23],[24],[25].

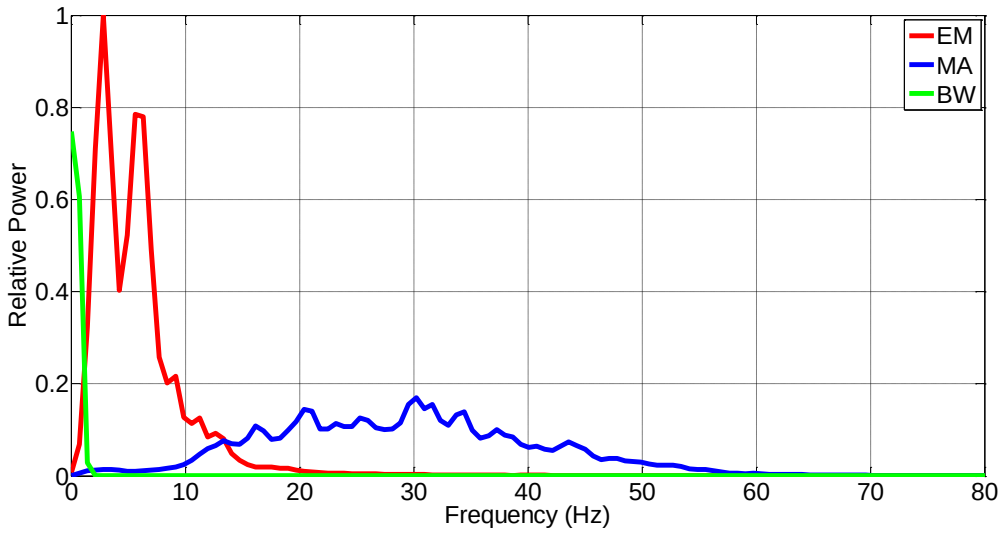

Figure 2.18 – *Spectral distribution of main noise types found in an ECG.*

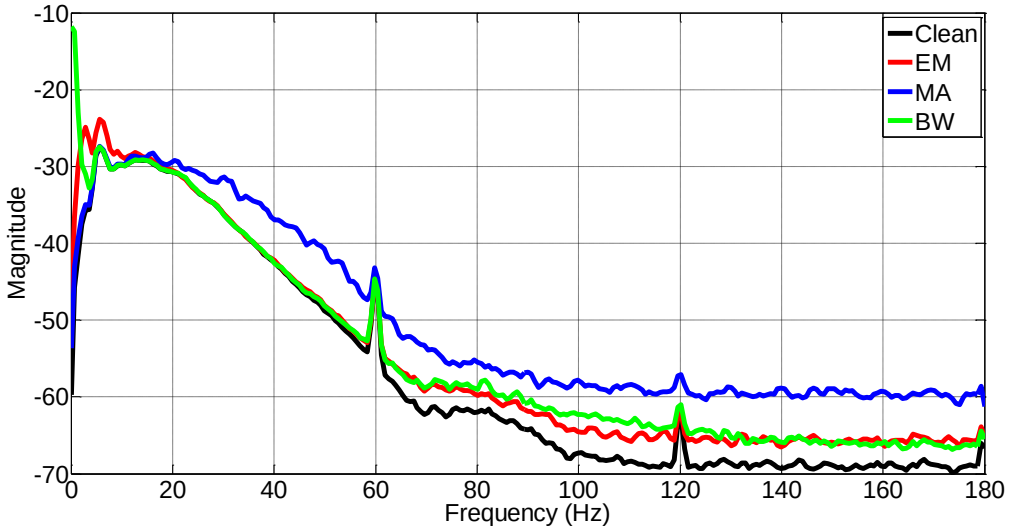

Figure 2.19 – *Magnitude of the spectral distribution of the signals contaminated with the different noise types comparing to the clean ECG.*

2.3.4 Noise treatment in ECG

One of the strategies used to control the impact of artifacts consists in the removal of noise periods when these are detected [4], [26]–[31].

In [31], before the separation of sources, the neguentropy (a gaussianity measure), is used to evaluate the presence of noisy segments.

In [30], a morphological filtering is performed in order to extract the EMG from the signals. As the influence of the QRS complexes is still present in the extracted vector, a suppression of these peaks is performed by reducing the magnitude by one-tenth on the corresponding periods. Finally, the detection of EMG noise presence is computed by thresholding the result of the moving variance on the EMG extracted and QRS suppressed vector. In [28] the use of accelerometers is explored in order to detect movement artifacts caused by corporal position changes.

In [4], noise detection is performed by extracting statistical metrics, namely the mean, variance and entropy, from the first Intrinsic Mode Function (IMF) obtained using the Empirical Mode Decomposition (EMD).

In [29], statistical properties are explored using the Laplacian model of the ECG signal. In [27], the Root Mean Square (RMS) error is calculated between the original signal and the approximation resulted from the reconstruction by Principal Component Analysis (PCA).

In [26], a set of detectors, each one being specific to a given type of noise, is explored. The signal overall quality is weighted by the effects of each type interference.

Another strategy is the reduction/cancelation of noise in the ECG rather than discarding the noisy periods [24], [31]–[33]. In [31], the Independent Component Analysis (ICA) is used to separate the clean ECG signal from the noise sources. In [24], denoising of ECG is performed resorting to a notch filter, and also to Wavelet and Empirical Mode Decomposition (EMD) methods. In [32], adaptive filtering is used for noise cancellation. In [33], a reduction of noise is performed by smoothing the signal with a Savitzky-Golay filter.

Chapter 3 – Noise Detection in PCG signals

In this chapter we are going to describe our low-complex and real-time processing methodology in noise detection periods for posterior removal.

3.1 Data acquisition

Multi-channel acquisitions occurred in two distinct populations, using different sensors and protocols. A detailed description is presented in the following subsections.

3.1.1 Healthy dataset

The PCG signals were acquired in a group of 23 healthy young subjects, that agreed with data acquisition and processing under anonymous conditions. There is a total of 370 minutes of PCG signals available for analysis. In order to evaluate the detection capabilities of the algorithm, subjects had to follow a defined protocol involving the deliberate/intentional production of noise during acquisitions. Three types of noise were induced along the signals: ambient, physiological and vocal noise (see **Figure 3.1**). For each subject we repeated two times the acquisition of one continuous signal for each noise type, leading to the recording of a total of six PCGs per subject.

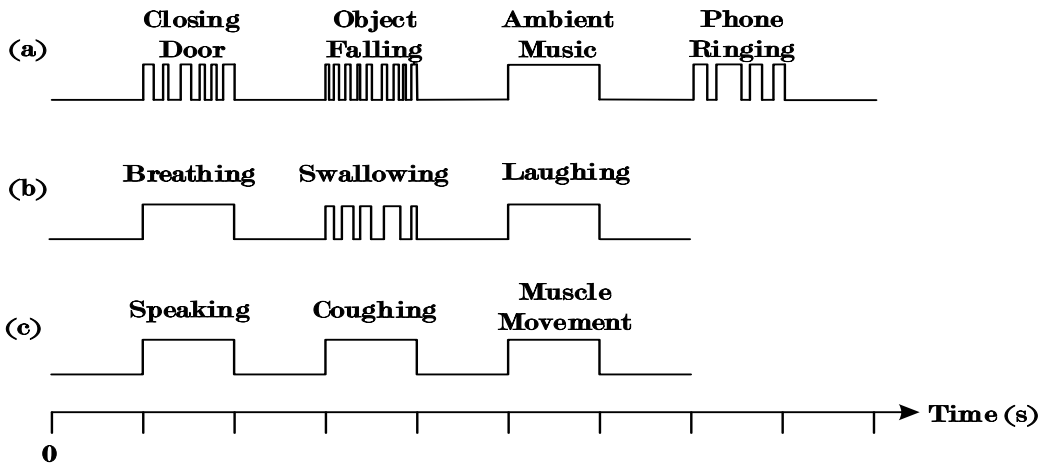

Figure 3.1 – *Acquisition protocol, a) corresponds to the signal corrupted with ambient noise, b) signals with the addition of physiological noise, and c) corresponds to signals induced with vocal noise. In some acquisitions clean and noisy segments lasted for 20s, in others they lasted 10s.*

The PCG signals were recorded using the data logger Sensatron (Philips, Eindhoven, Netherlands) with a sampling frequency of 4000Hz. The two microphones were placed in the pulmonary and mitral auscultation sites, as presented in **Figure 3.2**.

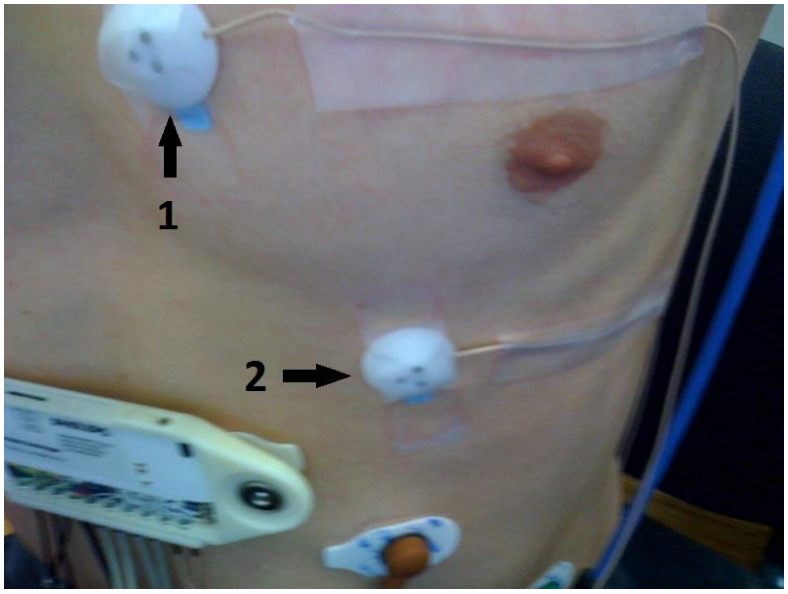

Figure 3.2 *– Experimental setup. The arrows 1 and 2 are pointing to the microphones placed at the pulmonary and mitral auscultation sites, respectively.*

3.1.2 Pathological dataset

These signals were acquired at the Coimbra University Hospital (HUC) from only subjects with heart conditions. The dataset comprises of 8 signals acquired in 8 subjects, accumulating 12 minutes of PCG signals. The signals were acquired in an uncontrolled hospital environment where noise is mainly originated due to abrasion of the stethoscopes with the skin and external voices. Data were acquired recurring to digital stethoscopes Meditron and by considering a sampling frequency of 2000 Hz. The stethoscopes were placed at the tricuspid and pulmonary auscultation sites.

3.2 Methods

Two main goals were envisaged for the development of the algorithm. In first place, it should be accurate and in second place it should be computationally efficient and process data in real-time, enabling integration in tele-monitoring systems. A diagram that generally depicts the algorithm is presented in **Figure 3.3**.

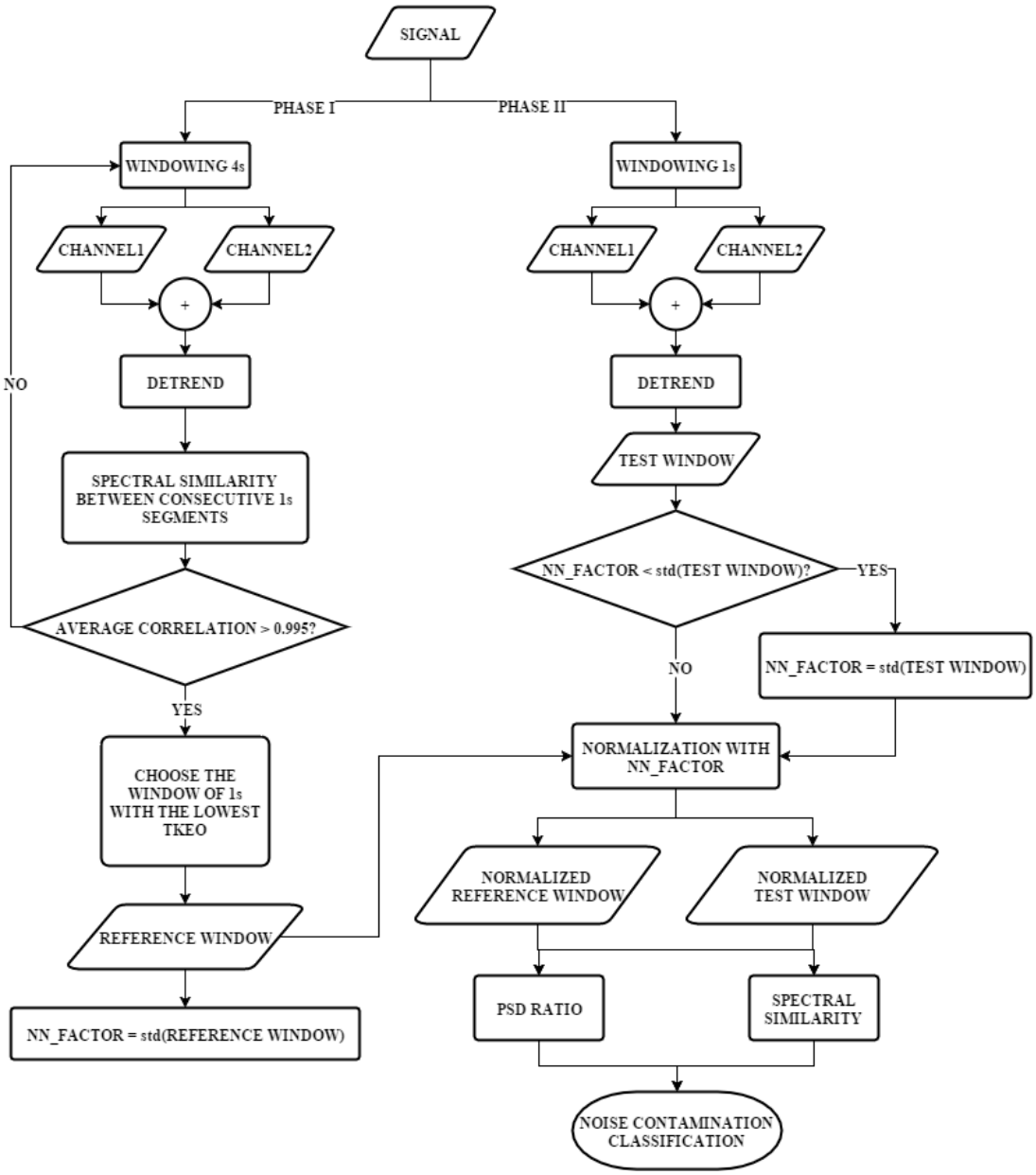

Figure 3.3 *– Diagram of the multi-channel approach (MCA) noise detection algorithm in PCG.*

The proposed algorithm can be divided in two phases: in the first phase there is a search for a noise free window to be used as a template of a clean HS epoch; the second phase uses the template as a reference window to compare with the test windows, and assess about the presence of noise. The features chosen to compare test and reference windows were based on spectral differences and greater amounts of high frequency components in the contaminated segments (see **Figure 2.6**, **Figure 2.7**, and **Figure 2.8**).

3.2.1 Phase I

In the first phase, the two PCGs from both channels, are windowed in 4s frames with an overlap of 70%. In each 4s window the two channels are summed and the resulting mean is subtracted to the signal.

$$S_W = s_W^{channel1} + s_W^{channel2} \quad \textbf{3.1}$$

$$S_W^d = S_W - mean(S_W) \quad \textbf{3.2}$$

In Equation **3.1**, $\boldsymbol{s_W^{channel1}}$ and $\boldsymbol{s_W^{channel2}}$ correspond to each channel signal in each 4s window, and their summation is given by $\boldsymbol{S_W}$. $\boldsymbol{S_W^d}$ in Equation **3.2** corresponds to the detrended $\boldsymbol{S_W}$ signal in each window. To evaluate if a certain 4s window is a proper candidate to look for a 1s reference window, the algorithm looks for a high spectral similarity between different segments present in the window. So, we segment the 4s window in 4 segments, each with 1s and no overlap, $\boldsymbol{C_k}$ (see **Figure 3.4**).

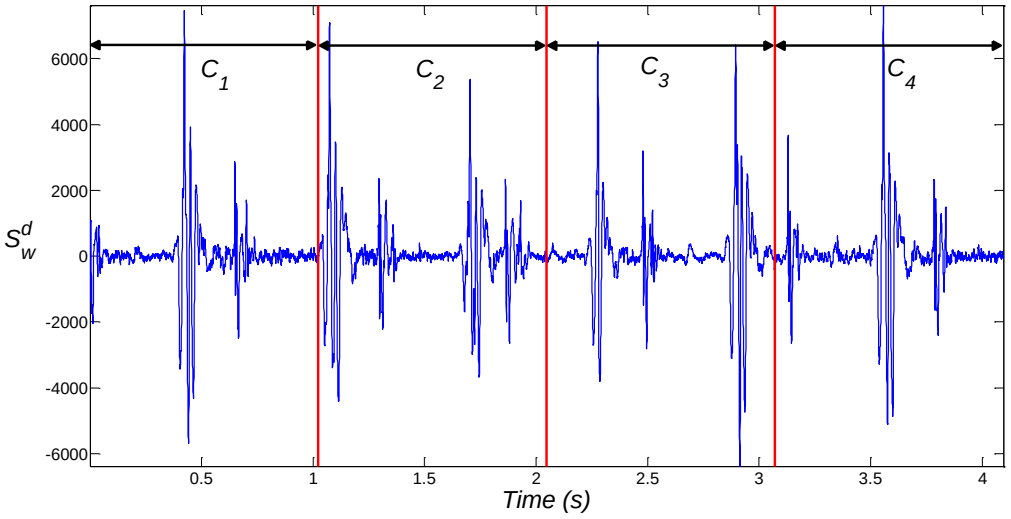

Figure 3.4 – *Example of a 4s window divided in 1s segments.*

Now, with the different segments separated, we can calculate the spectral similarity between them. This computation of spectral similarity was already used in [3] and [15]. To obtain the spectral distribution of each 1s segment, we recur to the

Discrete Time Short-Time Fourier Transform (DTSTFT), Equation **3.3**. The DTSTFT divides the signal in time intervals, and in each one performs the Discrete Fourier Transform (DFT). The final result is a matrix composed by the distribution of the frequency components in each temporal trajectory.

$$DTSTFT[m,k] = \sum_{n=1}^{N-1} x[n]w[n-m]e^{-2\pi ikn} \quad \textbf{3.3}$$

In Equation **3.3**, $\boldsymbol{DTSTFT[m,k]}$ is the DTSTFT of the signal $\boldsymbol{x}$ with $\boldsymbol{N}$ samples, and $\boldsymbol{w}$ is a window function. The $\boldsymbol{k}$ variable corresponds to a specific frequency with a total of $\boldsymbol{K}$ frequency trajectories, $\boldsymbol{m}$ to a time trajectory with a total of $\boldsymbol{M}$ trajectories, and $\boldsymbol{n}$ to a sample of the signal.

We perform the DTSTFT of each $\boldsymbol{C_k}$ using a Hanning window function with a span of 8ms and 50% of overlap between consecutive windows. The spectral distribution ($\boldsymbol{SD_k}$) of $\boldsymbol{C_k}$, given by Equation **3.4**, is obtained by the summation of the $\boldsymbol{DTSTFT_k}$'s magnitude along the $\boldsymbol{M}$ temporal trajectories and further calculation of the Root Mean Square (RMS) of that sum (see **Figure 3.5**).

$$SD_k[k] = \sqrt{\frac{1}{M}\sum_{m=1}^{M}(20log_{10}(|DTSTFT[m,k]\,|))^2} \quad \textbf{3.4}$$

Recurring to the example of **Figure 3.4**, the spectral distributions of the different segments are illustrated in **Figure 3.5**.

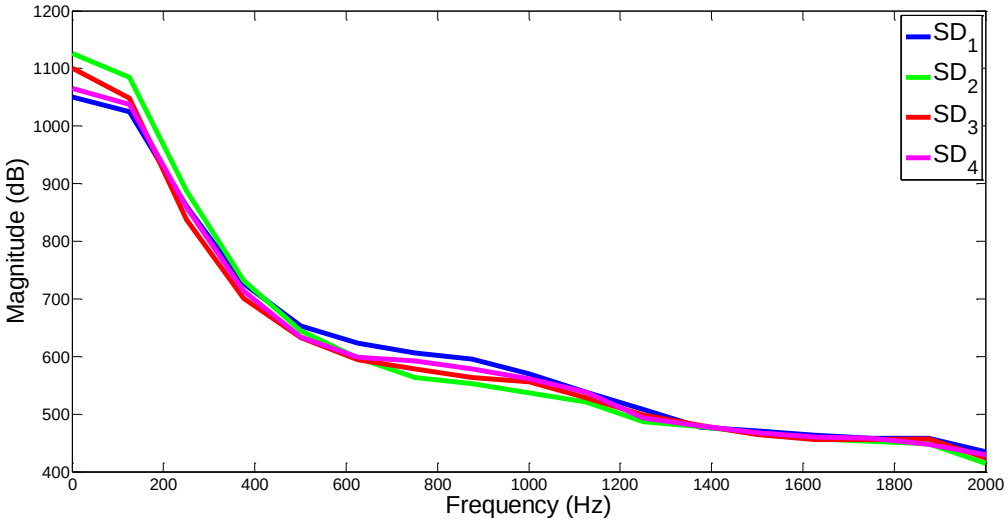

Figure 3.5 – *Spectral distribution of the different 1s segments present in the 4s window. In this case we have a spectral similarity of 0.9976.*

To measure the spectral similarity between the different segments, the Pearson Correlation Coefficient, Equation **3.5**, is computed for each pairwise $\boldsymbol{SD_k}$ combination.

$$Corr_{XY} = \frac{cov(X,Y)}{\sigma_X \sigma_Y} \qquad \textbf{3.5}$$

In Equation **3.5**, $\boldsymbol{cov}$ corresponds to the covariance of two variables, and $\boldsymbol{\sigma}$ the standard deviation. If the average correlation is greater than 0.995, than it is assumed that the 4s window is a proper candidate to find a clean reference window. If not, the algorithm analyses the next 4s window with 70% of overlap. The value of 0.995 for average correlation, was taken by using this methodology on the entire length of the training signals, and assessing the noise sensitivity it provided to us. This value was able to reach a noise sensitivity of 95%, in other words, it assures us a noise free 4s window with 95% of certainty.

Next, if the condition of the clean 4s window is met, there is a search of a 1s window to serve as a reference of a noise free window and compare it to the remaining 1s windows of the signal. The 1s reference window, $\boldsymbol{REF}$, is the one with the lowest overall Teager-Kaiser Energy Operator (TKEO), Equation **3.8**, present in the 4s window. Once the TKEO increases when high amplitude and frequency sounds are present, the

1s window with the lowest TKEO is going to correspond to the least probable window to contain noise artifacts. An example of a reference window is shown in **Figure 3.6**.

$$TKEO[n] = S_W^d[n]^2 + S_W^d[n-1]S_W^d[n+1] \quad \textbf{3.6}$$

$$REF_{inds} = n \ \ where: \ \ min\left\{\sum_{n=2}^{n+fs} TKEO[n], \ldots, \sum_{n=L_S-fs}^{L_S-1} TKEO[n]\right\} \quad \textbf{3.7}$$

$$REF = S_W^d[REF_{inds}] \quad \textbf{3.8}$$

To conclude Phase I, the standard deviation of the reference window is calculated (see Equation **3.9**). This value ($\boldsymbol{NN_{Factor}}$) will be used as a normalization factor for the test windows.

$$NN_{Factor} = \sigma_{REF} \quad \textbf{3.9}$$

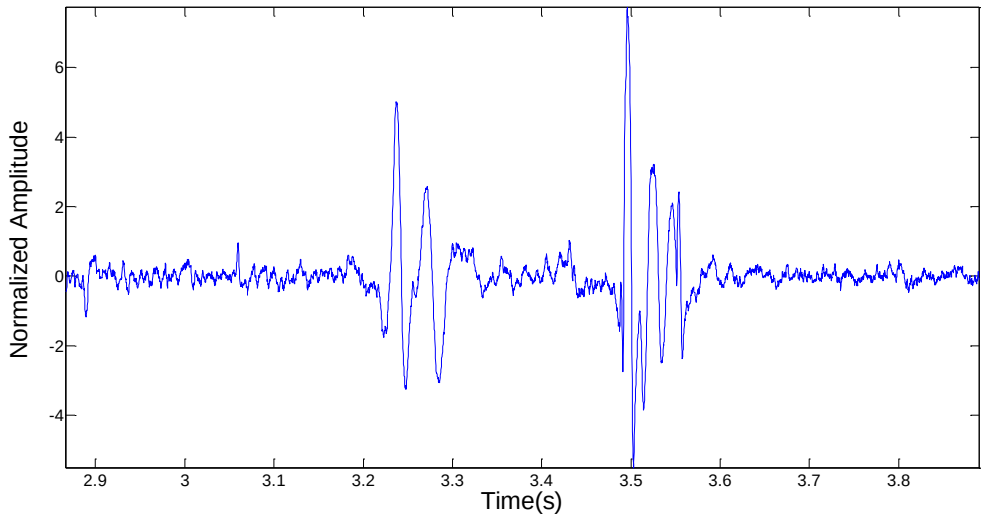

Figure 3.6 – *An example of a reference window.*

3.2.2 Phase II

In this second phase, we frame the PCG signal in 1s windows with 80% overlap, beginning at the end of the reference window. This 1s windows are the ones that are going to be assessed about the presence of noise artifacts, therefore, called test windows. In each test window the preprocessing is similar to the one performed in first

phase, namely a summation of the two channels and the respective detrend (see Equation **3.1** and **3.2**). After that, the test window and the reference window are normalized with the $\boldsymbol{NN_{Factor}}$ obtained in the first phase. This $\boldsymbol{NN_{Factor}}$ is updated if the standard deviation of the current test window is greater than the previous value.

$$REF^{norm} = \frac{REF}{NN_{Factor}} \quad \textbf{3.10}$$

$$TEST = \left(s_{test}^{channel1} + s_{test}^{channel2}\right) - mean(s_{test}^{channel1} + s_{test}^{channel2}) \quad \textbf{3.11}$$

$$TEST^{norm} = \frac{TEST}{NN_{Factor}} \quad \textbf{3.12}$$

Finally, to ascertain about the presence of noise artifacts, two features are computed, using the reference and test windows: the spectral similarity (see Equation **3.15**), and the High Frequencies Power Spectral Density (HFPSD) ratio ($\boldsymbol{HF_{ratio}}$) (see Equation **3.19**).

$$SD_{ref}[k] = \sqrt{\frac{1}{M}\sum_{m=1}^{M}(20log_{10}(|STFT_{REF^{norm}}[m,k]\,|))^2} \quad \textbf{3.13}$$

$$SD_{test}[k] = \sqrt{\frac{1}{M}\sum_{m=1}^{M}(20log_{10}(|STFT_{TEST^{norm}}[m,k]\,|))^2} \quad \textbf{3.14}$$

$$R = Corr_{SD_{test}SD_{ref}} \quad \textbf{3.15}$$

The $\boldsymbol{HF_{ratio}}$ corresponds to the ratio between the total amount of high frequency components (higher than $\boldsymbol{Fc}$ Hz) in the reference and test window. The DFT (see Equation **3.16**) is used to compute the Power Spectral Density (PSD) of a given window (see Equation **3.17**).

$$Y_w[k] = \sum_{n=1}^{N-1} x[n]w[n]e^{-2\pi ikn} \quad \textbf{3.16}$$

$$PSD_w[k] = \frac{1}{fsL}|Y_w[k]|^2 \quad \textbf{3.17}$$

$$HFPSD_w = \sum_{k=Fc\cdot L/f_N}^{L} PSD_w[k] \quad \textbf{3.18}$$

$$HF_{ratio} = \frac{HFPSD_w^{test}}{HFPSD_w^{ref}} \quad \textbf{3.19}$$

Now, having the two features computed we apply a threshold technique to evaluate about the presence of noise contamination (see Condition **3.20**).

$$IF \quad R < R_{th} \quad OR \quad HF_{ratio} > HF_{th} \quad \rightarrow \quad Noise\ Contamination \quad \textbf{3.20}$$

In Condition **3.20**, $\boldsymbol{R_{th}}$ corresponds to threshold of the spectral similarity $\boldsymbol{R}$, and $\boldsymbol{HF_{th}}$ to the threshold of $\boldsymbol{HF_{ratio}}$ feature.

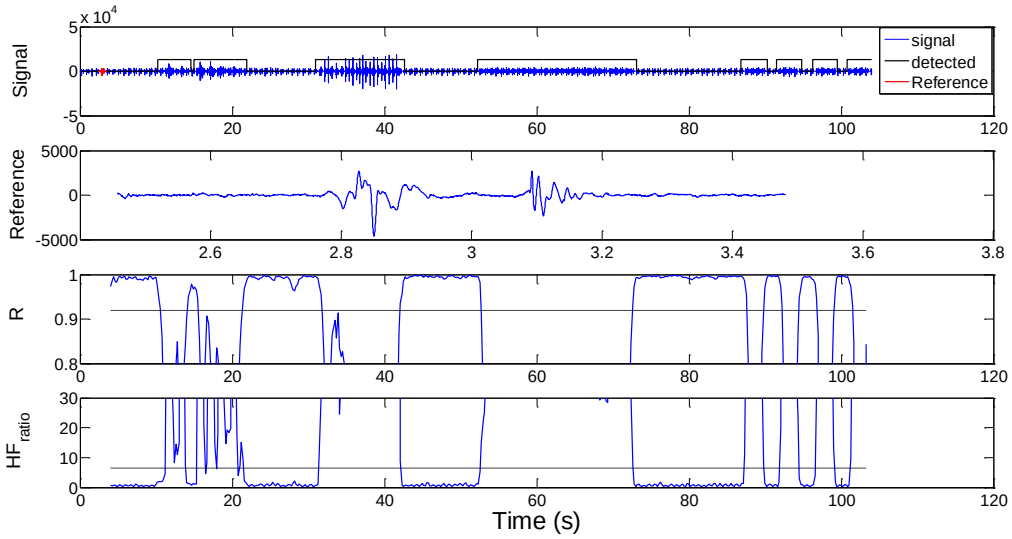

Figure 3.7 – *Algorithm's noise detection result, and the respective reference and features result. The set of parameters* $\boldsymbol{R_{th}}$, $\boldsymbol{HF_{th}}$ *and* $\boldsymbol{Fc}$ *were set to 0.92, 6.5 and 170, respectively.*

3.3 Results

3.3.1 Tuning phase

To train the algorithm we used signals from six different subjects from the healthy dataset, which has a total of 35 signals, sampled at 4000Hz. The best parameter combination, namely $\boldsymbol{R_{th}}$, $\boldsymbol{HF_{th}}$ and $\boldsymbol{Fc}$, was found recurring to a Receiver Operating Characteristic (ROC) analysis. The optimal combination was given by the highest module of mean sensitivity and specificity on the training dataset. The best parameter combination correspond to a mean sensitivity and specificity of 95.31% and 93.76% (see **Figure 3.8**). The results for each subject and noise type are presented in **Table 3.1**.

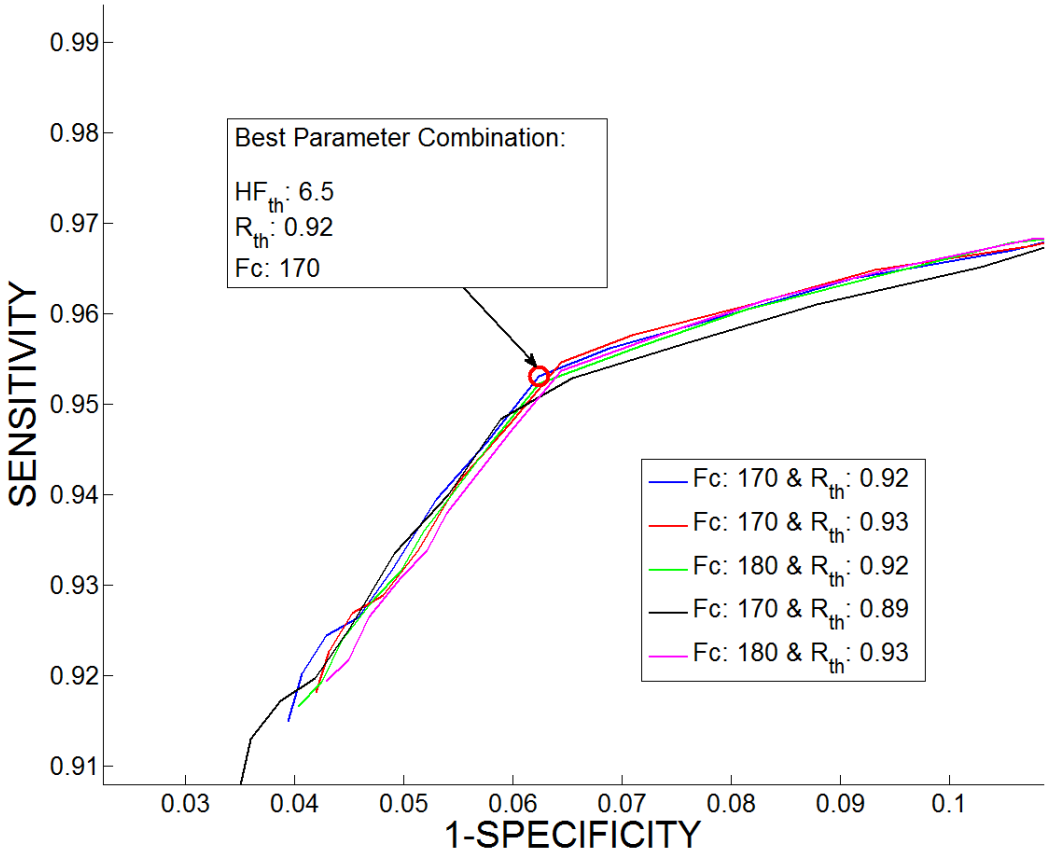

Figure 3.8 – *ROC curves for the different parameter combinations in the training dataset.*

Table 3.1 – *Noise sensitivity (SS) and specificity (SP) for all the signals in training dataset.*

ID	Age	BMI (Kg/m²)	Run	Noise Type					
				Ambient		Physiological		Vocal	
				SS (%)	SP (%)	SS (%)	SP (%)	SS (%)	SP (%)
1	35	28,01	1	99,13	91,11	100,00	86,75	98,57	93,79
			2	97,82	96,17	87,92	89,85	99,94	91,79
2	28	22,47	1	97,86	99,12	90,90	89,44	99,93	97,54
			2	93,16	100,00	89,56	90,65	99,74	98,35
3	33	25,11	1	100,00	91,39	97,35	93,04	-	-
			2	100,00	89,12	43,66	97,38	93,89	91,26
4	30	16,65	1	99,16	96,77	88,30	98,06	100,00	95,08
			2	99,00	98,84	90,05	100,00	100,00	99,76
5	24	21,51	1	99,45	96,48	98,22	71,40	99,68	95,73
			2	99,62	94,94	89,61	96,98	100,00	75,58
6	28	22,91	1	100,00	95,44	89,99	94,32	100,00	95,51
			2	100,00	97,40	93,74	96,05	99,63	96,50
Average per Noise Type				98,77	95,57	88,27	91,99	99,22	93,72

It is important to refer that the framing methodology that was used, in the frontiers of noisy periods, is going to result in windows classified as noise where there are both noise and clean samples. The algorithm was trained to not count as false positives the clean samples present in a given window where both classes (clean and noisy) of HSs are present. This was made in order to explore the full capabilities of the algorithm on the noise detection. If we chose not to do this procedure, the lower specificity due to the false positives present in a window with contaminated samples, would result in an increase of the thresholds to compensate the low specificity and thus, affecting our noise sensitivity. To conclude, we are imposing to the training methodology that it is fine to classify a window as noise contaminated when this window has noise periods. The results presented in **Table 3.1** and **Figure 3.8** are computed by having this in account.

Although the algorithm has been trained to not count false positives in windows where both classes (noisy and clean) are present, in a real situation these false positives must be counted, as it discards clean periods, which might contain valuable information. If we count the false positives at the margins of the noise periods, we get a mean

specificity of 85.88%, a drop of 7.88%. Although the decrease in specificity is not critical, we have to take into account the entire length of the signal being analyzed. In the case of the training dataset, the signals have a considerable high duration, comparing to the assessment window duration, which results in a small drop of the specificity. However, if we had signals with half the duration, this effect would be much more prominent, as the false positives within a detected window would represent a higher percentage of the signal - which is the case of the testing healthy dataset, where the different tasks have only 10 seconds instead of 20 seconds of the training data. This problematic is shown **Figure 3.9**.

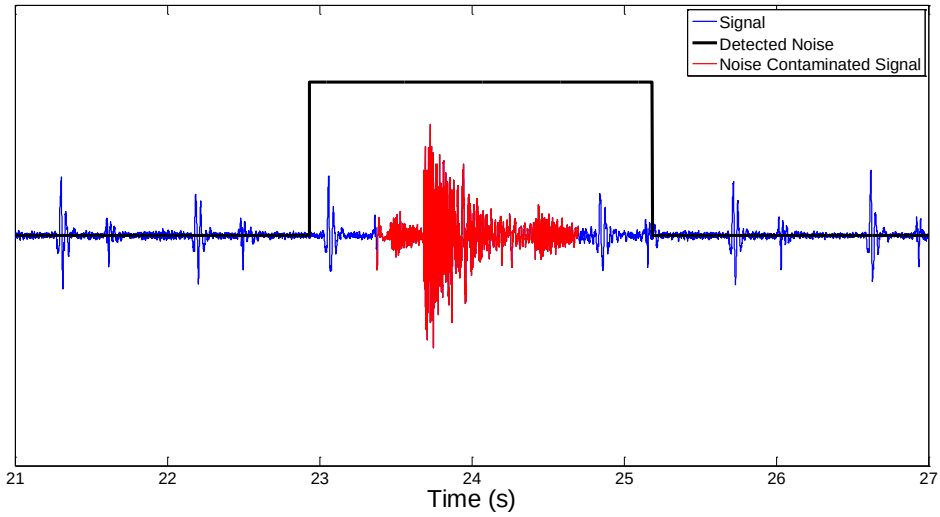

Figure 3.9 – *Noise detection on a contaminated period (door closing).*

This problem consists in a resolution problem of the framing methodology. We could reduce the length of the analyzing 1s window, however it would result in a loss of robustness, as it would most probably result in a reference window without at least one HS cycle, and cause comparison problems between the reference and clean test windows.

To overcome this resolution problem, maintaining the 1s window, the following methodology is used. In each 1s window only the central 20% of the actual window (which is renewed in each frame with 80% of overlap) is going to be classified as a noisy or clean. A scheme that better describes this resolution narrowing is depicted in Appendix A.

Recurring to the example of **Figure 3.9** the result of the narrowing methodology, or high resolution approach, is depicted in the following figure.

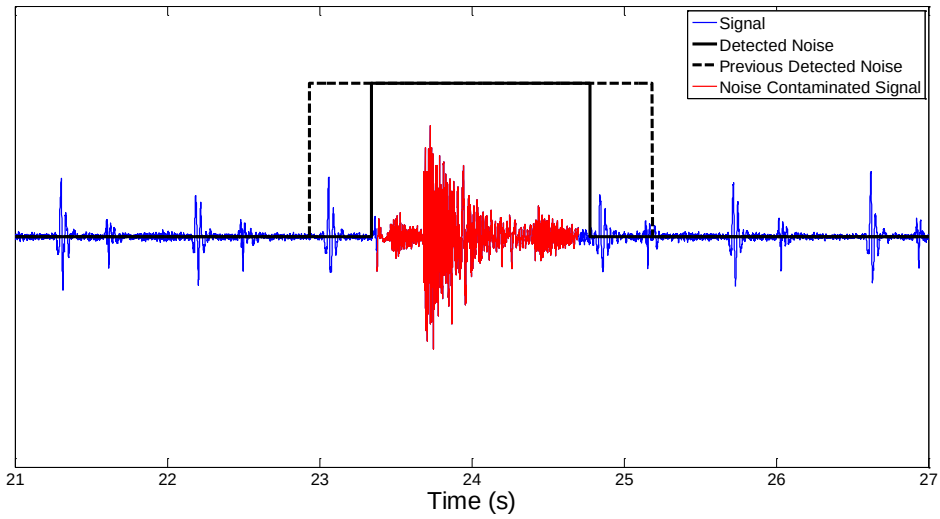

Figure 3.10 – *Differences between the different detection techniques.*

The results on the training dataset for the high resolution approach were 83.08% and 95.72% of mean sensitivity and specificity, respectively. Although it resulted in a trade-off of sensitivity for specificity, it provides us a higher independency regarding to the signal duration. The decrease in sensitivity may be explained by the fact that some large blocks of noise were annotated as one entire noise period, which increases the count of false negatives due to the presence of small clean segments between the noisy periods, as confirmed visually.

3.3.2 Testing phase

3.3.2.1 Healthy dataset

The healthy testing dataset comprises of 17 subjects, accounting for a total of 51 PCGs (six per subject) and has a total of 280 minutes of signal. The multi-channel approach was tested using the set of parameters found in the training phase. The noise sensitivity and specificity results for the testing dataset are presented in **Table 3.2**.

Table 3.2 – *Noise sensitivity (SS) and specificity (SP) for all the signals in the healthy testing dataset. Each value of sensitivity and specificity, corresponds to mean value of the two runs for each subject and noisy type.*

ID	Age	BMI (Kg/m^2)	Sex	Ambient		Physiological		Vocal	
				SS (%)	SP (%)	SS (%)	SP (%)	SS (%)	SP (%)
7	24	18,59	F	96,97	91,79	76,43	98,06	95,52	93,89
8	24	25,01	M	97,52	94,77	77,42	93,11	98,58	94,46
9	23	18,72	M	92,87	97,10	92,99	98,23	97,03	84,55
10	24	19,59	M	94,33	95,73	97,63	93,06	98,43	90,57
11	24	21,88	M	96,25	86,11	77,12	62,73	91,82	80,22
12	24	21,88	M	94,07	95,24	54,68	98,90	89,12	81,25
13	22	25,31	M	95,97	92,32	85,88	95,91	95,90	85,57
14	25	21,89	M	93,17	92,54	93,98	88,55	95,58	88,27
15	24	22,99	M	99,66	85,85	83,29	85,31	99,36	82,63
16	19	21,47	M	91,98	96,35	83,29	97,82	95,05	91,90
17	24	24,62	M	98,45	92,89	96,12	93,55	87,88	85,20
18	24	21,55	M	94,11	90,24	94,81	92,48	89,37	95,96
19	21	20,98	M	93,97	90,81	70,59	97,56	88,85	76,84
20	22	23,30	M	97,90	92,32	92,85	93,86	97,68	88,10
21	22	25,14	M	98,91	91,91	90,52	94,27	98,41	85,53
22	24	22,79	M	98,05	94,81	85,38	90,06	95,88	85,31
23	24	23,90	M	81,36	96,61	87,11	98,57	83,40	95,28
Average per Noise type				95,03	92,79	84,71	92,47	93,99	87,38

The multi-channel approach returns 91.24% and 90.88% of mean sensitivity and specificity, respectively. We also tested this dataset for the signals downsampled to 2000 Hz, the results of the algorithm were 88.48% and 91.02% for mean sensitivity and specificity, respectively.

The single channel approach (SCA) was also compared with other single-channel methods, namely the Periodicity-based (PB) algorithm [3] and the Modulation Filtering (MF) algorithm [2]. We have chosen these algorithms for comparison based on its documented high precision and code availability. The results are presented in **Table 3.3** and **Table 3.4.**

Table 3.3 – *Results corresponding to the signals acquired in the Mitral auscultation site for the different single-channel algorithms, for each noise type. The* ***Time*** *row corresponds to the processing time in seconds, each algorithm takes to analyze one minute of PCG signal with a sampling frequency of 4000Hz. These results were computed using MATLAB version R2013b and a 4.00GHz Intel Core i7-4790k processor.*

Mitral	SCA		MF		PB	
	SS (%)	SP (%)	SS (%)	SP (%)	SS (%)	SP (%)
Ambient	93,64	94,00	84,92	52,46	97,10	89,13
Physiological	79,69	91,81	75,32	56,74	75,45	83,74
Vocal	86,22	92,56	96,26	47,28	86,54	75,09
Average	86,51	92,79	85,50	52,16	86,36	82,65
Time (s)	0,17		0,82		0,32	

Table 3.4 – *Results corresponding to the signals acquired in the Pulmonary auscultation site for the different single-channel algorithms, for each noise type.*

Pulmonary	SCA		MF		PB	
	SS (%)	SP (%)	SS (%)	SP (%)	SS (%)	SP (%)
Ambient	95,19	91,23	86,46	39,12	94,67	81,70
Physiological	81,10	90,04	73,49	41,48	79,55	77,25
Vocal	94,03	87,04	97,35	35,30	93,10	69,46
Average	90,11	89,43	85,77	38,63	89,11	76,14

3.3.2.2 Pathological dataset

We used the entire pathological dataset for test. The Multi-Channel Approach results are presented in the following table.

Table 3.5 – *Results of sensitivity and specificity for each subject on the pathological dataset using the multi-channel approach algorithm.*

ID	Age	Sex	BMI	SS (%)	SP (%)	Condition
1	82	M	23,8	97,09	70,67	Cardiac Insufficiency Class 3; Ischemic Cardiopathy
2	78	M	28,4	70,39	93,88	Cardiac Insufficiency Class 1; Valvular disease; Coronary Disease
3	69	M	28,7	70,86	95,31	Cardiac Insufficiency Class 3; Mitral Insufficiency
4	81	F	18,7	100,00	94,65	Cardiac Insufficiency
5	71	M	30,9	50,00	96,08	Cardiac Insufficiency Class 3; Coronary Disease;
6	84	M	23,7	53,96	97,78	Cardiac Insufficiency; Ventricular Dysrhythmia
7	82	M	23,7	76,09	97,59	Submitted to Aortic Arch Surgery
8	81	F	22,2	97,70	87,44	Cardiac Insufficiency Class 2;
Average				77,01	91,68	

Comparison of the SCA algorithm with the other single-channel algorithms is presented in **Table 3.6**.

Table 3.6 – *Results for each auscultation site, for the different single-channel algorithms in the pathological dataset.*

	Pulmonary		Tricuspid	
	SS (%)	SP (%)	SS (%)	SP (%)
SCA	88,20	87,20	84,30	90,86
PB	72,40	84,29	61,53	82,27
MF	79,68	55,80	81,51	48,29

3.4 Discussion

Looking at the results in **Table 3.3**, **Table 3.4** and **Table 3.6**, it can be seen that the SCA presents the highest mean sensitivity and specificity between all the analyzed algorithms, as also the least computational time. The reason lies in its simplicity, which provides the algorithm with robustness, generalization capabilities and low

processing times. The physiological noise was the most difficult to detect among all the tested algorithms, which can be due to the lower amplitudes and frequency components this noise type presents.

A reason to justify the low specificity of the MF algorithm in the healthy and pathological testing dataset, is the use of a 3s window to assess the noise periods, causing a resolution problem. In the pathological dataset in addition to the resolution problem, the MF algorithm may also have false detections due to the pathological HS, as referred by the authors [2].

The PB algorithm presents a high sensitivity, however a lower specificity in general, mainly due to resolution problems. The lower specificity in vocal noise, comparing to the specificity in the signals with ambient and physiological noise, is due to the differences in amplitude between the reference and the test windows, as some tasks, e.g. coughing, laughing, may increase the heart rate, and result in the increase of energy in the HS. As one of the features for noise classification in the PB algorithm is the energy ratio between reference and test windows, this increase in heart rate, and consequently its energy, may result in false detections.

The different methodologies were tested in pathological signals in order to infer if the algorithms were sensitive to murmurs or other abnormal HSs. The high specificity of the MCA and SCA indicates that the two approaches are able to differentiate between pathological events from noisy periods.

The lower sensitivities in the pathological dataset compared to the ones in the healthy dataset is due to the lower number of noisy periods along the signals, and thus, not having a sufficient noise duration in each signal to infer with certainty about each algorithm's ability to detect noise. Other factor that influences the lower sensitivity is that the acquisitions were made in a controlled and silent ambient, causing the involuntary noise periods to have a low amplitude.

The results for the MCA and SCA prove the utility and efficacy of the developed methodology. However, in a multi-channel situation, one may ask why not apply the single-channel approach in each channel and join the final results, for a multi-channel

resolution. In fact, the sum of the different channels is expected to result in an amplification on the noise artifacts, as the noise sources will affect both channels. This can be seen by the slightest better results of the MCA (see **Table 3.2**) comparing the results of the SCA (see **Table 3.3** and **Table 3.4**). Additionally, the computational time, is reduced to half by using the MCA, an important asset to implement in tele-monitoring systems.

The pathological dataset was acquired using two stethoscopes, each handled by an individual subject, and the major noise source of this acquisitions was the abrasion between the skin and stethoscopes, resulting on the independency of noise presence between channels. Therefore, the usage of the SCA is a more suitable approach for this situation, as we can compare by the results of the MCA and SCA, in **Table 3.5** and **Table 3.6**, respectively.

3.5 Concluding remarks

A fast and reliable algorithm has been developed, being suitable for integration in real-time in a multi or single-channel acquisition system. Future work may include:

- Increasing the number of subjects of the healthy and pathological testing datasets in order to see the performance that the algorithm achieves in a dataset that better depicts the overall population, and the diversity of cardiovascular diseases;
- Testing the methodology on signals that weren't conditioned by any acquisition protocol or a controlled environment, to inspect about its performance in a real-life situation;
- Assessment of the improvement in the detection of cardiac pathologies, after the noisy periods detected by the MCA have been discarded from further analysis.

Chapter 4 – Noise Detection in ECG signals

In this chapter we will describe an algorithm developed to detect noise periods on single-lead ECG signals for quality evaluation. This algorithm had the finality to be integrated in the WELCOME (http://www.welcome-project.eu) vest, a tele-monitoring system, from the project of the same name. It was optimized to match the characteristics of the referred system, namely, ECG signals at a sampling frequency of 250Hz, and 5 minutes of duration.

4.1 Data

We used the ECG signals available from Physionet (MIT-BIH Arrhythmia Database - http://physionet.org/physiobank/database/mitdb), and noise records from the MIT-BIH Noise Stress Database also from Physionet (http://physionet.org/physiobank/database/nstdb/), all with a sampling frequency of 360Hz. The noise records were acquired in a way that the subject's ECG signals were not visible. Three types of noise were derived from these records, the baseline wondering (BW), the electromyogram (EMG) artifact (MA), and the electrode motion artifact (EM) (see **Figure 4.1**).

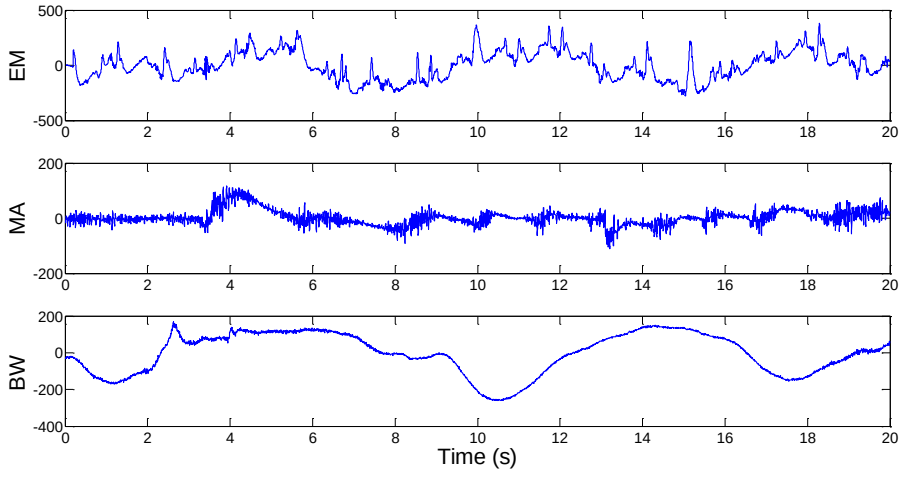

Figure 4.1 – *Segments of the noise records from Physionet used to add noise to the signals at different SNR's. EM corresponding to the electrode motion noise in the 'em' record of Physionet. MA corresponding to the muscle noise in the 'ma' record. And BW corresponding to the baseline wandering noise in the 'bw' record.*

To add the noise to the ECG signals at different SNR's, we used the 'nst' function from the WFDB Software Package also provided by Physionet (http://physionet.org/physiotools/wfdb.shtml), based on a peak to peak amplitude to compute the gains to apply to the noise records.

The MIT-BIH Arrhythmia Database possess a total of 46 signals of lead MLII, 40 of V1, 4 of V2, 1 of V4, and 5 of V5, most of them with a high degree of arrhythmias prevalence. We only used the signals with a high quality, i.e., the signals with few natural noise periods. This selection was made to prevent the adverse effect of having noise periods left to annotate, and thus, affecting the algorithm's specificity, and also with the objective of having a better insight about the algorithm capabilities on detecting different noise types at different SNR's, which we computationally added. So, we ended up with a total of 25 signals of lead MLII (625 minutes), 21 of lead V1 (525 minutes), 4 of lead V2 (100 minutes), and 5 of lead V5 (125 minutes).

With the chosen dataset, we divided it in two subsets, one for training, and another for test of the developed algorithm. We trained our algorithm on 6 different signals of lead MLII, namely the records 201, 205, 213, 217, 223 and 231, comprising in a total of 150 minutes. We have chosen these records due to its high quality signal and the presence of various types of arrhythmias, in order to determine the parameters that best discriminate the noise periods, keeping a low sensitivity to arrhythmia patterns.

The three noise types were added to the dataset at 6 different SNR levels, namely -6, 0, 6, 12, 18 and 24 dB, like depicted in **Figure 4.2**.

To match the sampling frequency used in the WELCOME vest, all the signal were down sampled to 250 Hz recurring to the Piecewise Cubic Hermite Interpolating Polynomial (PCHIP).

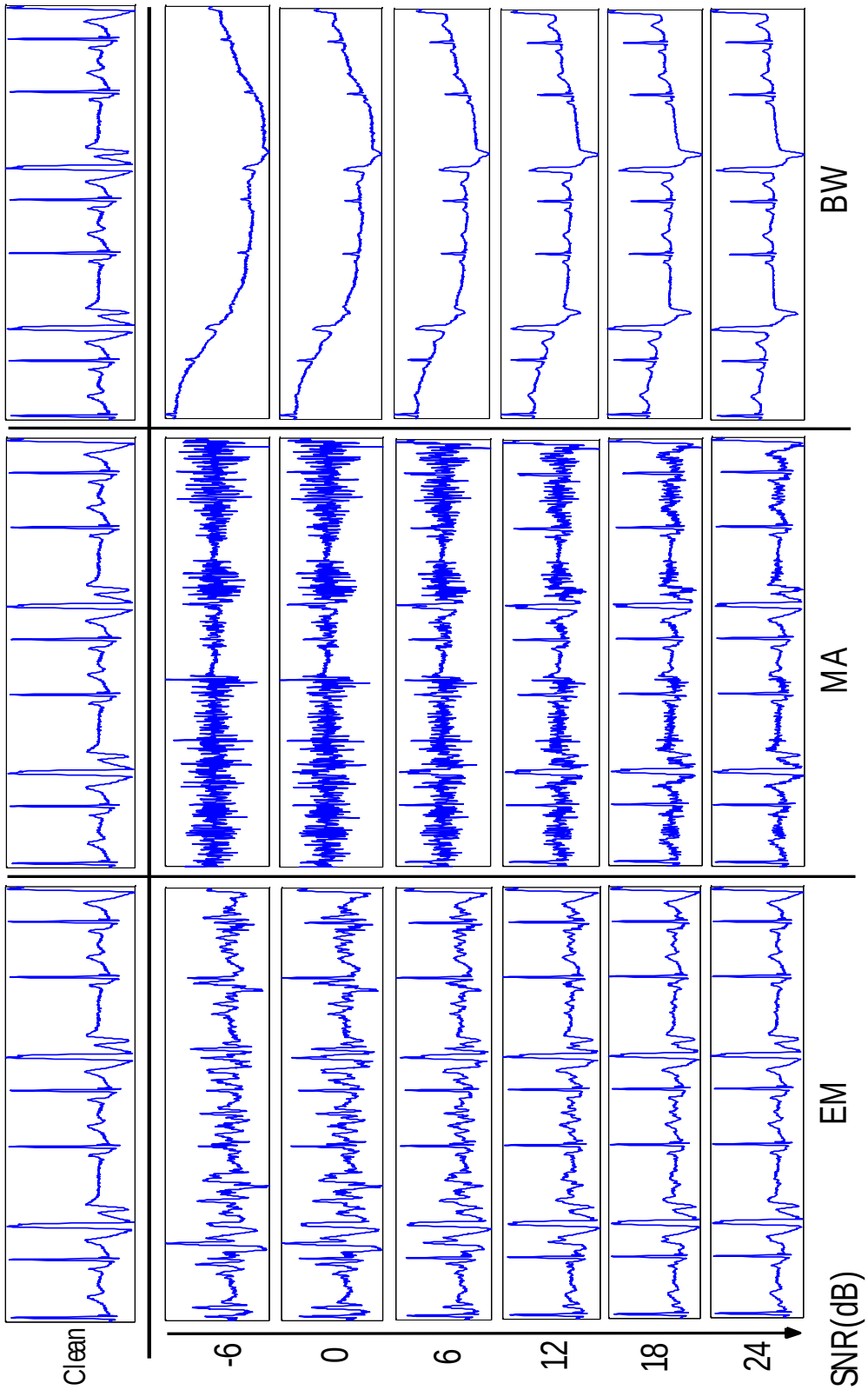

Figure 4.2 – *The effect that each noise type produces in a clean ECG segment at different SNRs.*

4.2 Methods

The focus of this algorithm is the detection of noise periods in multi-lead ECG signals, and depending on the amount and duration of the noise periods, evaluate about the signal quality. We choose to not implement a reduction noise strategy since the amount of available ECG signal is plenty, and the referred strategy might distort the original signal and lose valuable information. So we choose to adopt the strategy of removing the noisy periods as for PCG. A diagram that generally depicts the algorithm is shown in **Figure 4.3**. The algorithm was designed with the aim of high adaptation for different leads. The total noise detection method comprehend four main stages:

- The preprocessing stage where the baseline shifts are removed and the signal is normalized.
- An R-peak detection stage.
- The stage where the two features, the approximation error by PCA and the result of a High Frequency Filtering used for classification are derived.
- A final stage where the assessment of noise corruption is performed in 4 seconds windows recurring to the main features.

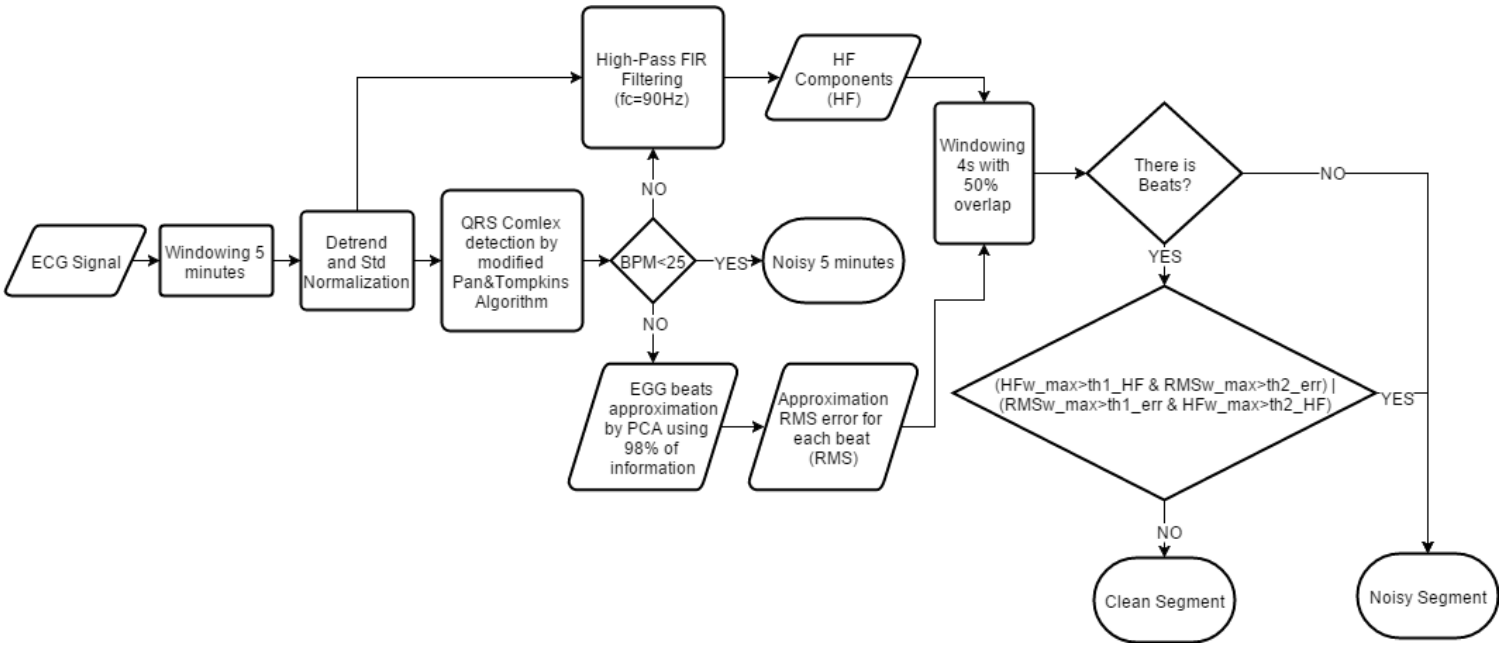

Figure 4.3 – *Diagram of the noise detection algorithm in ECG.*

4.2.1 Preprocessing

The algorithm was optimized for 5 minutes segments of ECG signal, thus, each signal must last for at least 5 minutes. If the signal is longer than 5 minutes, the signal is windowed for that time. During each 5 minutes segment, it is removed the baseline drift from the signal recurring to a high-pass FIR filtering (see Equation **4.1**), with a cut-off frequency of 0.5 Hz [25] and an order of 100. Then, that signal is normalized using his standard deviation.

$$S^d = S[n] * B[m] \qquad n = 1, \dots, L_S; \quad m = 1, \dots, L_b + 1 \tag{4.1}$$

$$S_n^d = \frac{S^d}{\sigma_{S^d}} \tag{4.2}$$

In Equation **4.1**, $\boldsymbol{S^d}$ is the result of the signal S with a length of $\boldsymbol{L_S}$ convoluted by the high-pass filter $\boldsymbol{B}$ with an order of $\boldsymbol{L_b}$, and $\boldsymbol{S_n^d}$ in Equation **4.2** is the detrended and normalized signal.

4.2.2 R-peak detection

In order to obtain the beat matrix to perform the approximation by PCA in the next stage, first we must segment the ECG according to each heartbeat. To do so, we use a R-peak detector based on the Pan & Tompkins Algorithm [34]. In order to detect the R-peaks, it is performed a band-pass filtering between 5 and 20 Hz ($\boldsymbol{S^f}$), then the energy ($\boldsymbol{E}$) of the signal is derived with the square of the first derivative (see Equation **4.3**). The energy is then smoothed by a moving average (MA) filter with a span of 2 seconds (see Equation **4.4**).

$$E[n] = (S^f[n+1] - S^f[n])^2\,, \qquad n = 1, \dots, L_S - 1 \tag{4.3}$$

$$E^s[n] = \frac{1}{2fs} \sum_{n-fs}^{n+fs} E[n]\,, \qquad n = 1 + fs, \dots, L_S - fs \tag{4.4}$$

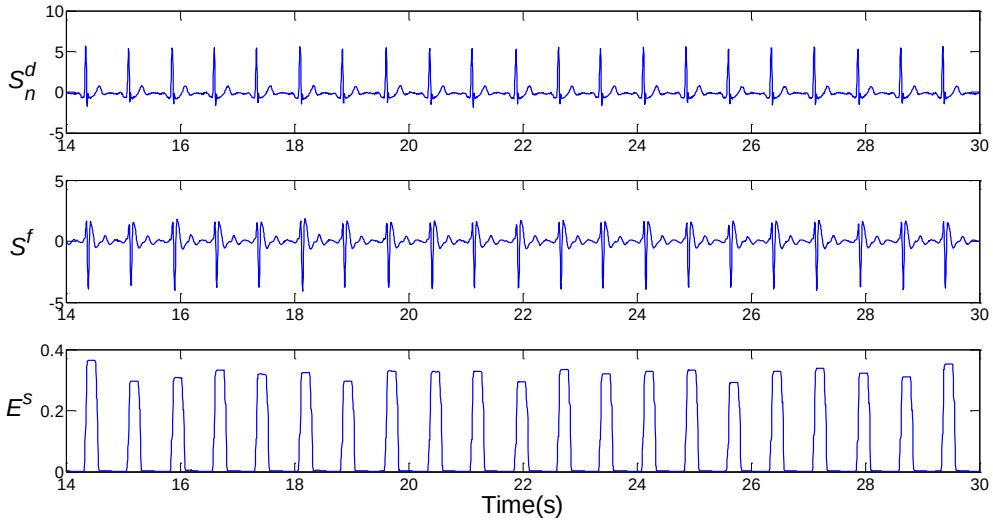

Figure 4.4 – *Envelope computation of the ECG beats.*

The modification performed in this algorithm is in the threshold to assess the peaks locations, which is adaptive. The threshold is derived by the result of a moving average filter with a span of 2 seconds on the resulted energy vector. This modification is made to take in account the individuality of each subject and lead, and on the different possible beat amplitudes in the same signal, like depicted in **Figure 4.5**.

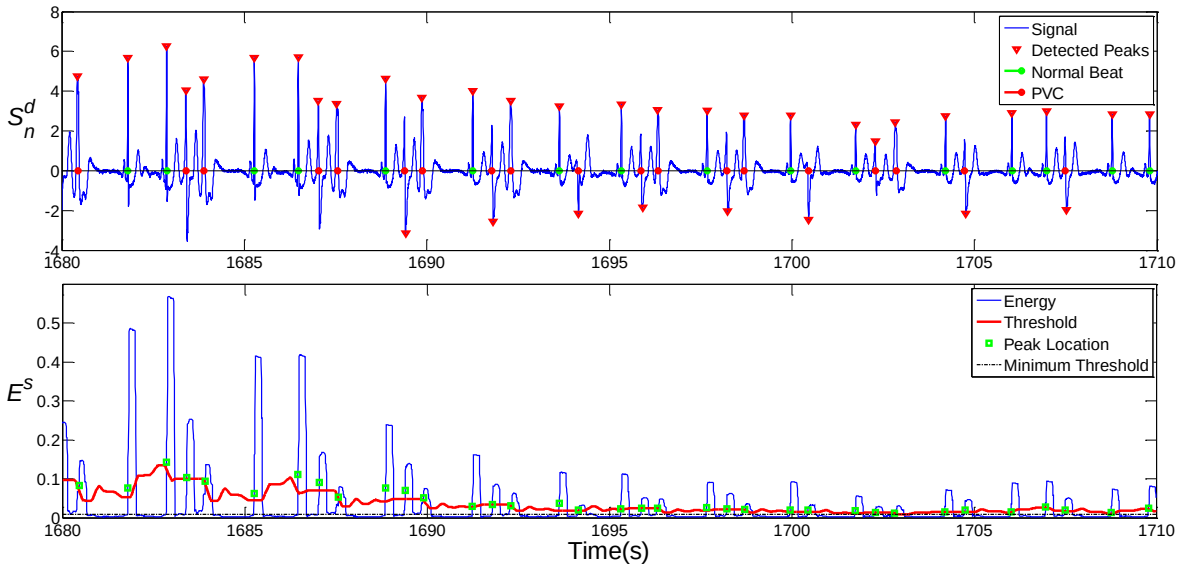

Figure 4.5 – *Different amplitude beats, and the threshold variation.*

The peaks location on each energy peak envelope are going to be the first sample higher than the threshold. As the process of filtering causes a phase shift compared to the initial signal, the real peak locations are assessed by finding the absolute maximum

on the original signal around 150ms from the energy peaks locations. Then, there is a removal of the peaks corresponding to an RR interval less than 100ms.

The adaptability of the moving average threshold provides us a great sensibility in R-peaks on different types of signal. But, in the case of a lead-off period, the threshold, due to its characteristics, is automatically going to meet the zero energy baseline, and detect peaks where it is not supposed to detect. So, to prevent this effect, a minimum value threshold is needed, see **Figure 4.6**.

To compute the minimum threshold value, we first calculate the Zero-Crossing Rate (ZCR) in each 2 second window with 0% overlap, i.e., the rate at which the signal crosses the zero line. The goal is to find in which signal windows, beats are present or not. A lead-off window is expected to have a ZCR around or superior to 50 (due to the electromagnetic interference of 50Hz or 60 Hz). While a non-lead-off window is expected to have a ZCR inferior than 50. So, within the periods with a ZCR inferior than 40, we calculate the mean energy amplitude value of the corresponding periods, i.e., the periods with beats. The minimum threshold is then computed as in Equation **4.5**.

$$th_{min} = E_{min} + 0.1(A_{mean} - E_{min}) \quad \textbf{4.5}$$

In Equation **4.5**, $\boldsymbol{th_{min}}$ corresponds to minimum threshold value, $\boldsymbol{E_{min}}$ to the minimum value on the energy vector $\boldsymbol{E}$, and $\boldsymbol{A_{mean}}$ to the mean energy value of the periods with a ZCR inferior than 40.

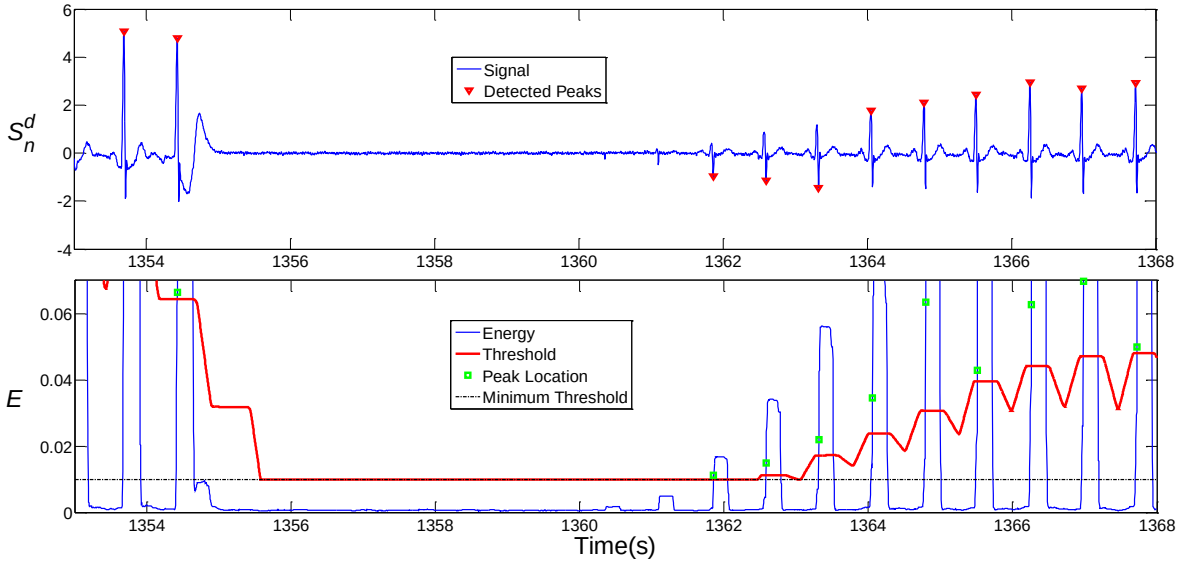

Figure 4.6 – *Plot of a lead-off period (1355s - 1361s).*

If the rate of beats per minute is less than 25, the whole 5 min are considered as non-quality signal. This because the physiological impossibility of this heart rate, indicates a disconnection of the electrodes from the skin.

4.2.3 Root mean square error of the approximation by PCA

The PCA will be performed on the beat matrix (***M***), which consist in one beat per line. Each beat $\boldsymbol{B_i}$ in ***M*** is obtained from the adjacent R-peaks locations of the current R-peak location, $\boldsymbol{R_i}$ (see Equation **4.6** and **4.7**). As the lengths of each beat are different we must perform a resampling to equalize all the beat lengths in order to perform the PCA. The chosen length is 125 samples. All the beats in ***M*** suffer a min-max normalization (see **Figure 4.7**).

$$B_i^{reach} = min\left\{\frac{R_i - R_{i-1}}{2}, \frac{R_{i+1} - R_i}{2}\right\} \quad \textbf{4.6}$$

$$B_i = S_n^d[k], \quad k = R_i - B_i^{reach}, \ldots, R_i + B_i^{reach} \quad \textbf{4.7}$$

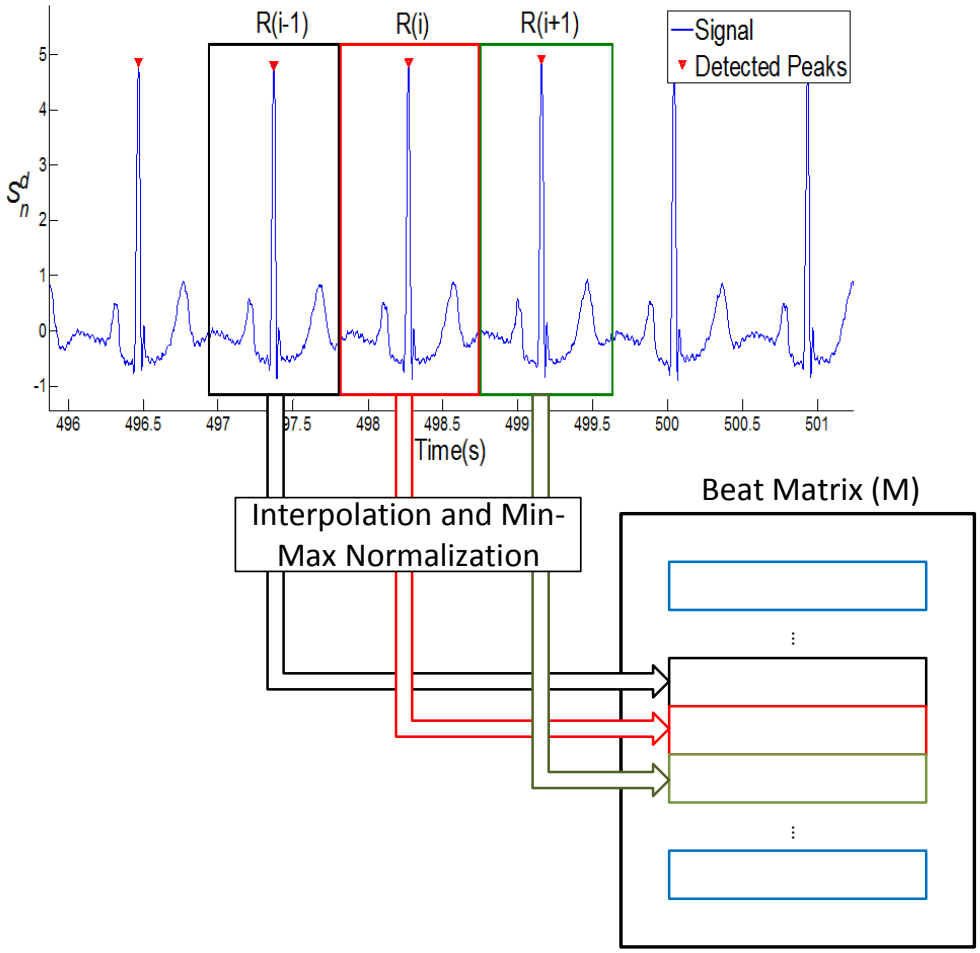

Figure 4.7 *– Illustration of how the beat matrix M is computed.*

Then we derive the eigenvalues and the eigenvectors of the covariance matrix of $\boldsymbol{M}$, and make the reconstruction of the beats matrix based only on the eigenvectors that provide at least 98% of the initial total variance. This value was found as the best to discriminate between noise and clean periods according to a ROC analysis.

$$ApproxM = MVV^T \qquad \textbf{4.8}$$

In Equation **4.8**, the matrix $\boldsymbol{ApproxM}$ is the result of the reconstruction of $\boldsymbol{M}$ based only on the most significant eigenvectors, $\boldsymbol{V}$. $\boldsymbol{ApproxM}$ has the same size of $\boldsymbol{M}$, with $\boldsymbol{N}$ lines and 125 columns, corresponding to the number of beats and the beat lengths, respectively (see **Figure 4.8**).

$$RMS_{err}[i] = \sqrt{\sum_{j=1}^{fs/2} (ApproxM[i,j] - M[i,j])^2}, \quad i = 1, \dots, N; \quad j = 1, \dots, fs/2 \qquad \textbf{4.9}$$

In Equation **4.9**, the vector $\boldsymbol{RMS_{err}}$ is the root mean square error between the original beats and the approximation beats. This vector is one of the features used to assess the presence of noise in ECG segments, [27]. Finally, is smoothed with a MA filter.

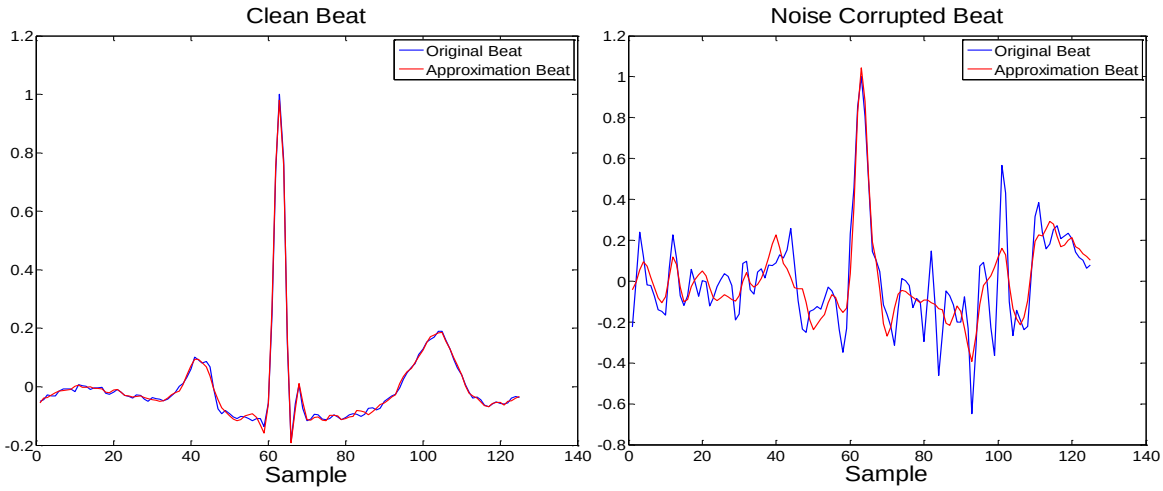

Figure 4.8 – *Comparison between the approximation by PCA of a clean heartbeat and a noise corrupted one.*

4.2.4 High-pass FIR filtering

The second feature to assess the presence of noise artifacts is the result of a high-pass FIR filter with a cut-off frequency (fc) of 90 Hz and an order of 100 (see Equation **4.1**). The fc of 90 Hz was found as the best to discriminate between noise and clean periods according to a ROC analysis. Finally, this feature is smoothed with a MA filter.

4.2.5 Noise assessment in 4s segments and thresholding

The assessment of corrupted periods is done by windowing the whole length of the signal in 4 seconds chunks with 50% of overlap, and examine the two features in that periods. Before the windowing, the thresholds must be determined to evaluate what is, and what is not noise. These thresholds are not fixed to specific values, they change in

each analyzed signal. To set them, we must first look for noise free periods. The clean periods correspond to the 3 segments, each with 10 beats, with minimum $\boldsymbol{RMS_{err}}$ and no overlap. The average $\boldsymbol{RMS_{err}}$ of these segments is taken as our reference error for clean periods, $\boldsymbol{REF_{err}}$. The thresholds for the first feature are derived from this value as shown in Equation **4.10** and **4.11**.

$$th1_{err} = f1_{err} \cdot REF_{err} \quad \textbf{4.10}$$

$$th2_{err} = REF_{err} + f2_{err} \cdot (th1_{err} - REF_{err}) \quad \textbf{4.11}$$

In Equation **4.10** and **4.11**, $\boldsymbol{th1_{err}}$ and $\boldsymbol{th2_{err}}$ correspond to the adaptive thresholds for the first feature, $\boldsymbol{RMS_{err}}$. The $\boldsymbol{f1_{err}}$ and $\boldsymbol{f2_{err}}$ are constant values found in the training stage by ROC analysis and correspond to 2 and 0.5, respectively. To find the thresholds for the second feature, $\boldsymbol{HF_X}$, a similar methodology is taken. The same periods of time used to assess $\boldsymbol{REF_{err}}$ are used to calculate $\boldsymbol{REF_{HF}}$, which is the mean value of $\boldsymbol{HF_X}$ on those periods. The thresholds for the second feature are derived from this value as shown in Equation **4.12** and **4.13**.

$$th1_{HF} = f1_{HF} \cdot REF_{HF} \quad \textbf{4.12}$$

$$th2_{HF} = REF_{HF} + f2_{HF} \cdot (th1_{HF} - REF_{HF}) \quad \textbf{4.13}$$

The $\boldsymbol{th1_{HF}}$ and $\boldsymbol{th2_{HF}}$ correspond to the adaptive thresholds for the second feature, $\boldsymbol{HF_X}$. The $\boldsymbol{f1_{HF}}$ and $\boldsymbol{f2_{HF}}$ are constant values found in the training stage by ROC analysis and correspond to 1.115 and 0.6, respectively.

The reason to choose the $\boldsymbol{RMS_{err}}$ feature to look for clean periods lies in his highly sensitivity to noise. One might ask, why just not use this feature for classification if it is so noise sensitive. The reason is that it is also sensitive for uncommon heart beat types, which normally corresponds to abnormal heart beats and rhythms that we want to diagnose. On the other hand, the $\boldsymbol{HF_X}$ feature don´t discriminate between different heart beats or rhythm types, even if it hasn't the noise sensitivity of the first. The

combination of the two features and multiple thresholds give the algorithm a more founded decision rule to assess whether a 4s segment signal is noise corrupted or not. Before the final decision rule (see Condition **4.14**), in each 4s chunk is evaluated if there are beats detected by the R-peak detector, if not, the whole chunk is considered as non-quality segment.

$$
\begin{aligned}
&IF \ \{ \\
&(\max\{HF_X^w\} > th1_{HF} \ \text{ AND } \ \max\{RMS_{err}^w\} > th2_{err}) \\
&\text{OR} \\
&(\max\{RMS_{err}^w\} > th1_{err} \ \text{ AND } \ \max\{HF_X^w\} > th2_{HF}) \\
&\}
\end{aligned}
\qquad \textbf{4.14}
$$

In Condition **4.14**, $\mathbf{max}\{\boldsymbol{HF_X^w}\}$ and $\mathbf{max}\{\boldsymbol{RMS_{err}^w}\}$ represent the maximum values on the 4s window of the first and second feature, respectively. If the condition is true, then the whole window is classified as noise corrupted.

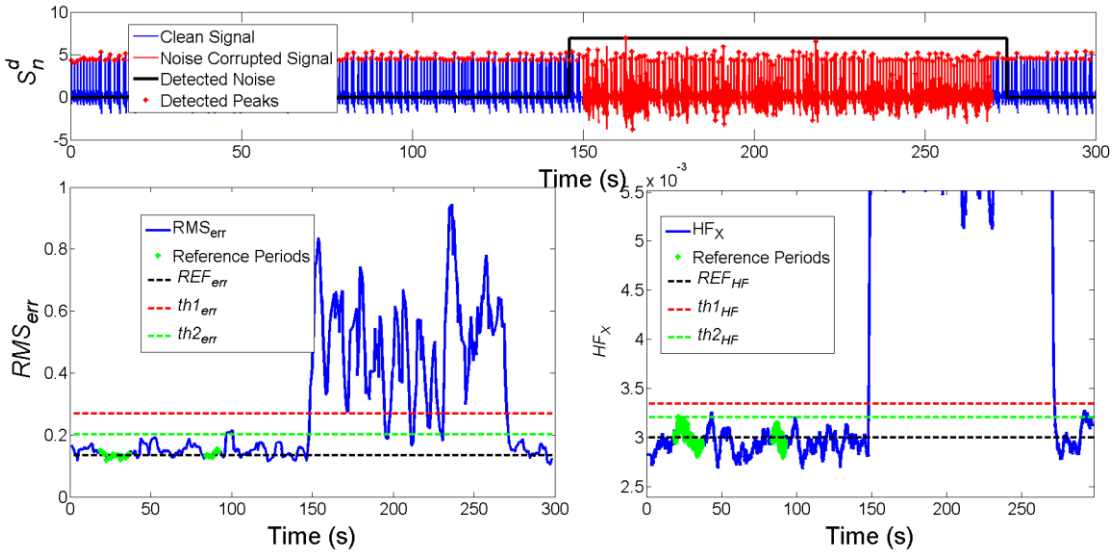

Figure 4.9 – *Result of the noise classification performed in an ECG signal with one noise corrupted period.*

4.3 Results

All the results were computed using MATLAB version R2013b and a 4.00GHz Intel Core i7-4790k processor. To see the influence that different noise types have on a detection algorithm, we tested our R-peak detection algorithm on the contaminated signals, see **Table 4.1**.

Table 4.1 – *Results on the influence that different noise types have on the R-peak detector at different SNR levels. These results were computed on the MLII test data. The results on the clean signals were **99.39%** and **99.64%** of sensitivity (SS) and specificity (SP), respectively. The average computational time is 0.01s per minute of ECG signal.*

SNR (dB)	EM		MA		BW	
	SS (%)	SP (%)	SS (%)	SP (%)	SS (%)	SP (%)
-6	36,17	27,41	36,82	34,20	88,86	51,19
0	63,47	43,42	47,48	47,03	95,57	79,24
6	91,28	67,26	63,40	60,70	98,31	92,38
12	98,55	92,30	86,29	73,38	99,26	97,76
18	99,31	98,98	96,90	84,33	99,38	99,34
24	99,37	99,44	99,30	97,36	99,38	99,54

To see the noise influence on an algorithm independent to the our noise detection algorithm, we tested the noise corrupted signals in another, more complex, R-peak detection algorithm, based on morphological transform to segment the different waves [35]. The result to sensitivity and specificity on the different noise contaminated signals are presented in **Table 4.2**.

Table 4.2 – *Results on the influence that different noise types have on the Morphological Transform R-peak detector at different SNR levels. These results were computed on the MLII test data. The results on the clean signals were **99.19%** and **99.99%** of sensitivity and specificity, respectively. The average computational time is 1.1s per minute of ECG signal.*

SNR (dB)	EM		MA		BW	
	SS (%)	SP (%)	SS (%)	SP (%)	SS (%)	SP (%)
-6	39,31	28,56	37,85	42,31	96,27	89,89
0	65,85	45,17	74,07	64,01	98,51	97,51
6	89,65	67,79	94,60	79,67	99,11	99,47
12	98,83	89,19	99,03	93,40	99,20	99,98
18	99,22	99,17	99,17	99,71	99,19	99,99
24	99,18	99,97	99,21	99,98	99,19	99,99

In the following table (**Table 4.3**), are presented the algorithm's results of sensitivity and specificity on the testing data.

Table 4.3 – *Results of mean sensitivity and specificity on the testing data at different leads and SNR levels.*

Lead	SNR (dB)	EM		MA		BW	
		SS (%)	SP (%)	SS (%)	SP (%)	SS (%)	SP (%)
MLII	-6	99,06	88,32	99,54	89,25	99,84	88,59
	0	99,27	89,04	99,60	89,26	99,61	88,59
	6	99,47	89,92	99,58	89,19	96,07	88,98
	12	98,92	90,37	98,44	90,37	75,85	91,39
	18	89,47	91,96	94,79	91,60	48,13	94,46
	24	63,05	92,73	82,17	92,14	26,17	95,38
V1	-6	99,42	87,73	99,73	87,71	99,50	88,25
	0	99,51	88,88	99,74	88,25	99,61	88,91
	6	99,19	89,04	99,58	88,25	96,62	88,17
	12	94,95	89,33	98,49	89,89	89,82	89,38
	18	77,53	89,79	94,24	89,93	55,28	92,74
	24	38,69	91,63	76,49	91,15	34,92	95,40
V2	-6	97,40	88,77	97,83	88,49	97,54	86,43
	0	97,75	89,47	98,12	88,54	97,73	87,64
	6	97,85	89,92	98,00	87,82	98,03	89,73
	12	96,81	90,33	98,07	88,48	92,22	89,80
	18	89,48	92,27	95,08	90,39	56,41	95,27
	24	55,04	94,61	82,18	93,68	33,45	95,61
V5	-6	96,55	90,42	100,00	88,47	99,74	89,58
	0	98,61	90,33	100,00	88,47	98,86	89,88
	6	97,78	90,76	99,01	88,70	91,71	92,29
	12	89,96	92,59	96,34	90,38	67,26	94,34
	18	70,91	93,90	88,39	93,51	34,51	96,09
	24	33,09	95,25	60,19	95,75	10,14	96,10
Total Average		86,66	90,72	93,98	89,99	74,96	91,38

One big problem in trying to assess noise contaminated periods in an ECG signal is that the algorithm may also detect abnormal heartbeats or rhythms as noise, and misclassify certain periods that are of great value for diagnose. Thus so, is essential to do a false positive analysis on the algorithm, and assess if the false positives are correlated with abnormal heartbeats or rhythms. As the algorithm is dependent of the whole signal being analyzed (due mainly to the $\boldsymbol{RMS_{err}}$ feature which takes 98% of information of

each signal) - and thus so, the algorithm's response in the clean periods for the same ECG may vary on the different noise types and SNR levels imposed – this false detection rate is the mean value for all the signals at different SNR levels and noise types. As the abnormal heartbeats have different manifestations on different leads, we did a false positive analysis on each lead as shown in the tables in Appendix B.

The only alarming result in the false positive analysis is the 78.87% detection rate on the supraventricular tachyarrhythmia rhythm in lead MLII. On the other hand, in the whole test dataset we only possess 14 seconds of this rhythm type in the clean periods, thus so, not having a sufficient statistical size to infer with certainty about the algorithm's sensitivity on this rhythm type.

4.4 Discussion

As we can see by the results of the two R-peak detector algorithms, the precision of both are very similar on the clean signals, however, the Morphological Transform (MT) based R-peak detector shows a slight higher robustness to noise compared to ours. These noise robustness comes with a cost, as we can see by the computational times. The computational cost of the MT algorithm is 2 orders of magnitude higher than our R-peak detector. However, is important to refer that the MT algorithm is capable of processing in real-time and besides the R-peaks detection, it also segments the P and T waves, and the QRS complex.

One may think that using an R-peak detector that fails at high degrees of noise on the segmentation of heartbeats is going to result in an adverse effect in the noise sensitivity of the $\boldsymbol{RMS_{err}}$ feature. However, it has the opposite effect on the noise detection context, as a wrong segmentation is going to produce a segment that completely differs from a typical heartbeat segment. As the PCA takes what is more common, when taking 98% of the information, these segments that resulted from the wrong segmentation, are going to have high approximation error, due to the nonsense of the segmentation.

This analysis on the R-peak detectors was with the intention to see the noise influence at different SNR levels on a determined ECG detection algorithm. Based on the results of **Table 4.1** and **Table 4.2**, we consider that the noise influence is only critical at [-6, 18] dB of SNR to the EM noise, [-6, 24] dB of to the MA noise, and [-6, 12] dB to the BW noise. The BW noise is less critical at higher SNR levels because this noise influence is easily overcame with the detrend of the ECG signal, a feature that the majority of ECG processing algorithms possess, and thus, being less troublesome [25]. The overall results to all leads were 94.08% and 89.88% of sensitivity and specificity, respectively, in the range of the SNR levels we assumed critical, as presented in the following table.

Table 4.4 – *Results for each lead and noise type at critical SNR levels.*

	EM [-6, 18] dB		**MA [-6, 24] dB**		**BW [-6, 12] dB**		**Average per Lead**	
	SS (%)	**SP (%)**	**SS (%)**	**SP (%)**	**SS (%)**	**SP (%)**	**SS (%)**	**SP (%)**
MLII	97,24	89,92	95,69	90,30	92,84	89,39	**95,26**	**89,87**
V1	94,12	88,95	94,71	89,20	96,39	88,68	**95,07**	**88,94**
V2	95,86	90,15	94,88	89,57	96,38	88,40	**95,71**	**89,37**
V5	90,76	91,60	90,66	90,88	89,39	91,52	**90,27**	**91,33**
Average per Noise Type	**94,49**	**90,16**	**93,98**	**89,99**	**93,75**	**89,50**	**94,08**	**89,88**
							TOTAL	

The results in the table above show us a high sensitivity and specificity on noise detection, and also that the precision of the algorithm does not vary much in different leads, suggesting a good adaptability for the different leads, which we intended from the beginning.

The highest precision documented in the literature is 96.63% and 94.74% of sensitivity and specificity, respectively, on the ECG noise detection context [4]. However, the authors only consider noise corruption in the periods where the R-peaks are not clearly recognizable, indicating that the documented precision is only correspondent for noise corrupted signals at very low SNR levels. The computational time of the referred algorithm is documented to be 0.2s per 5s of ECG signal at sampling frequency of 180Hz using MATLAB 2010a on 2.66GHz Intel Core2 processor. The computational time of our algorithm is 0.14s per 5 minute ECG signal with a sampling

frequency of 250 Hz, this using MATLAB version R2013b and a 4.00GHz Intel Core i7-4790k processor.

4.5 Concluding remarks

The noise detection algorithm in ECG demonstrates a high precision and a fast performance, as well as a good adaptability for different leads and high specificity even in pathological signals. The results indicate that it is a suitable algorithm to integrate in a Tele-monitoring system.

It was already integrated in the WELCOME vest to discard 5 minutes signals based on the amount of noise presence in the V2 lead, and also in the feature extraction server (processing cloud) to detect noise periods in all the 12 leads before the detection of Atrial Fibrillation is performed. We are waiting to see its performance in a real-life situation and its behavior in the leads that weren't analyzed, after the testing of the vest.

Chapter 5 – Conclusion

Our main objective was the noise detection in bio-signals, namely on PCG and ECG, recurring to fast and reliable noise detection algorithms.

In the PCG context we developed a high precision multi-channel (MCA) algorithm capable of real-time processing, as a single-channel approach (SCA) of the same. In comparison with the methodologies with the highest precision rates documented in literature, our algorithm achieved the best results in the same testing dataset, as also the best computational times. The MCA is suitable for integration when the noise sources influence is simultaneously present in both channels. When the noise influence is independent in each channel, the best integration would be the SCA, although the MCA also achieves a good sensitivity, as we can see in the pathological signals results in **Table 3.5** and **Table 3.6**.

In the ECG context, the developed algorithm also presented high precision and computational performance. In the ECG noise detection context, this analysis on various leads, noise types, SNR levels, and false positive correlation with pathology, was the most diverse analysis comparing to the ones found in literature. However, the ECG algorithm is conditioned and optimized for the WELCOME project characteristics. It would be interesting to develop a more general alternative algorithm without these restraints, and hopefully capable to process in a real-time situation, which also explores a multi-channel methodology. As soon as the WELCOME vest becomes available, we could explore these new methodologies based on the 12-lead ECGs, as also assess the performance of the developed single-channel algorithm in leads that weren't tested.

Considering the final result, we think that we met the proposed goals. In a next stage of the work, more bio-signals could be explored in the noise detection context, as the Respiratory Lung Sounds or the Electrical Impedance Tomography, which are also prone to noise contamination.

References

[1] J. R. Beard, A. Officer, I. A. de Carvalho, R. Sadana, A. M. Pot, J.-P. Michel, P. Lloyd-Sherlock, J. E. Epping-Jordan, G. M. E. E. (Geeske) Peeters, W. R. Mahanani, J. A. Thiyagarajan, and S. Chatterji, "The World report on ageing and health: a policy framework for healthy ageing," *Lancet*, Feb. 2016.

[2] J. P. Ramos, P. Carvalho, R. P. Paiva, and J. Henriques, "Modulation filtering for noise detection in heart sound signals," *Proc. Annu. Int. Conf. IEEE Eng. Med. Biol. Soc. EMBS*, pp. 6013–6016, 2011.

[3] D. Kumar, P. Carvalho, M. Antunes, R. P. Paiva, and J. Henriques, "Noise detection during heart sound recording using periodicity signatures.," *Physiol. Meas.*, vol. 32, no. 5, pp. 599–618, 2011.

[4] J. Lee, D. D. McManus, S. Merchant, and K. H. Chon, "Automatic motion and noise artifact detection in holter ECG data using empirical mode decomposition and statistical approaches," *IEEE Trans. Biomed. Eng.*, vol. 59, no. 6, pp. 1499–1506, 2012.

[5] M. Nichols, N. Townsend, P. Scarborough, and M. Rayner, "Cardiovascular disease in Europe 2014: epidemiological update," *Eur. Heart J.*, vol. 35, no. 42, pp. 2950–2959, 2014.

[6] Nichols Melanie, T. Nick, S. Peter, and R. Mike, *European Cardiovascular Disease Statistics*, no. September Issue. 2012.

[7] A. C. Norris, "Scope, Benefits and Limitations of Telemedicine," in *Essentials of Telemedicine and Telecare*, John Wiley & Sons, Ltd, 2001, pp. 19–38.

[8] C. U. Lehmann, E. Ammenwerth, and C. Nohr, *Studies in Health Technology and Informatics*. 2013.

[9] J. G. F. Cleland, A. a. Louis, A. S. Rigby, U. Janssens, and A. H. M. M. Balk, "Noninvasive Home Telemonitoring for Patients With Heart Failure at High Risk of Recurrent Admission and Death," *J. Am. Coll. Cardiol.*, vol. 45, no. 10, pp. 1654–1664, 2005.

[10] C. M. Lewandowski, N. Co-investigator, and C. M. Lewandowski, "Inquiry into Life," *Eff. Br. mindfulness Interv. acute pain Exp. An Exam. Individ. Differ.*, vol. 1, pp. 1689–1699, 2015.

[11] A. K. Abbas and R. Bassam, *Phonocardiography Signal Processing*, vol. 4. 2009.

[12] R. L. Watrous, "Computer-aided auscultation of the heart: From anatomy and physiology to diagnostic decision support," *Annu. Int. Conf. IEEE Eng. Med. Biol. - Proc.*, pp. 140–143, 2006.

[13] P. P-E, *Textbook in medical physiology and pathophysiology - essentials and clinical problems*. 2000.

[14] S. Rajan, R. Doraiswami, R. Stevenson, and R. Watrous, "Wavelet based bank of correlators approach for phonocardiogram signal classification," *Proc. IEEE-SP Int. Symp. Time-Frequency Time-Scale Anal. (Cat. No.98TH8380)*, pp. 77–80, 1998.

[15] P. Carvalho, P. Gilt, J. Henriques, L. Eugenio, and M. Antunes, "Low complexity algorithm for heart sound segmentation using the variance fractal dimension," *IEEE Int. Work. Intell. Signal Process. 2005.*, pp. 194–199, 2005.

[16] D. Barschdorff, U. Femmer, and E. Trowitzsch, "Automatic phonocardiogram signal analysis in infants based on wavelet transforms and artificial neural networks," *Comput. Cardiol. 1995*, pp. 753–756, 1995.

[17] A. S. Paul, E. a Wan, and A. T. Nelson, "Noise reduction for heart sounds using a modified minimum-mean squared error estimator with ECG gating.," *Conf. Proc. IEEE Eng. Med. Biol. Soc.*, vol. 1, pp. 3385–3390, 2006.

[18] Y. W. Bai and C. L. Lu, "The embedded digital stethoscope uses the adaptive noise cancellation filter and the type I Chebyshev IIR bandpass filter to reduce the noise of the heart sound," *Proc. 7th Int. Work. Enterp. Netw. Comput. Healthc. Ind. Heal. 2005*, pp. 278–281, 2005.

[19] M. Brusco and H. Nazeran, "Development of an Intelligent PDA-based Wearable Digital Phonocardiograph.," *Conf. Proc. IEEE Eng. Med. Biol. Soc.*, vol. 4, pp. 3506–3509, 2005.

[20] D. B. Foster, *Twelve-Lead Electrocardiography*, Second Edi. .

[21] R. J. Thozhal, "Automated ECG Analysis for Characteristics of Ischemia from Limb Lead MLIII Using the Discrete Hermite Transform," no. c, 2015.

[22] F. H. Netter, *Atlas of Human Anatomy*. Elsevier Health Sciences, 2010.

[23] G. Moody, W. Muldrow, and R. Mark, "A noise stress test for arrhythmia detectors," in *Computers in Cardiology*, vol. 11, 1984, pp. 381–384.

[24] R. Sivakumar, R. Tamilselvi, and S. Abinaya, "Noise Analysis & QRS Detection in ECG Signals," *2012 Int. Conf. Comput. Technol. Sci. (ICCTS 2012)*, vol. 47, no. Iccts, pp. 141–146, 2012.

[25] a B. M. A. Hossain and M. a Haque, "Analysis of Noise Sensitivity of Different ECG Detection Algorithms," vol. 3, no. 3, 2013.

[26] I. Jekova, V. Krasteva, I. Christov, and R. Abächerli, "Threshold-based system for noise detection in multilead ECG recordings," *Physiol. Meas.*, vol. 33, no. 9, pp. 1463–1477, 2012.

[27] R. Kher, D. Vala, and T. Pawar, "Detection of Low-pass Noise in ECG Signals," no. May, pp. 3–6, 2011.

[28] Y. Kishimoto, Y. Kutsuna, and K. Oguri, "Detecting motion artifact ECG noise during sleeping by means of a tri-axis accelerometer," *Annu. Int. Conf. IEEE Eng. Med. Biol. - Proc.*, pp. 2669–2672, 2007.

[29] A. Mincholé, L. Sörnmo, and P. Laguna, "ECG-based detection of body position changes using a Laplacian noise model," *Proc. Annu. Int. Conf. IEEE Eng. Med. Biol. Soc. EMBS*, vol. 14, pp. 6931–6934, 2011.

[30] P. Raphisak, S. C. Schuckers, and a. D. J. Curry, "An algorithm for EMG noise detection in large ECG data," *Comput. Cardiol. 2004*, vol. 1, no. 1, pp. 369–372, 2004.

[31] H. Yoon, H. Kim, S. Kwon, and K. Park, "An Automated Motion Artifact Removal Algorithm in Electrocardiogram Based on Independent Component Analysis," *Fifth Int. Conf. eHealth, Telemedicine, Soc. Med.*, no. c, pp. 15–20, 2013.

[32] M. Rahman, R. Shaik, and D. Reddy, "Noise Cancellation in ECG Signals using Computationally Simplified Adaptive Filtering Techniques: Application to Biotelemetry," *Signal Process. An …*, vol. 3, no. 5, pp. 120–131, 2009.

[33] C. So-In, C. Phaudphut, and K. Rujirakul, "Real-Time ECG Noise Reduction with QRS Complex Detection for Mobile Health Services," *Arab. J. Sci. Eng.*, 2015.

[34] J. Pan and W. J. Tompkins, "A real-time QRS detection algorithm.," *IEEE Trans. Biomed. Eng.*, vol. 32, no. 3, pp. 230–236, 1985.

[35] Y. Sun, K. L. Chan, and S. M. Krishnan, "Characteristic wave detection in ECG signal using morphological transform.," *BMC Cardiovasc. Disord.*, vol. 5, p. 28, 2005.

Appendix A

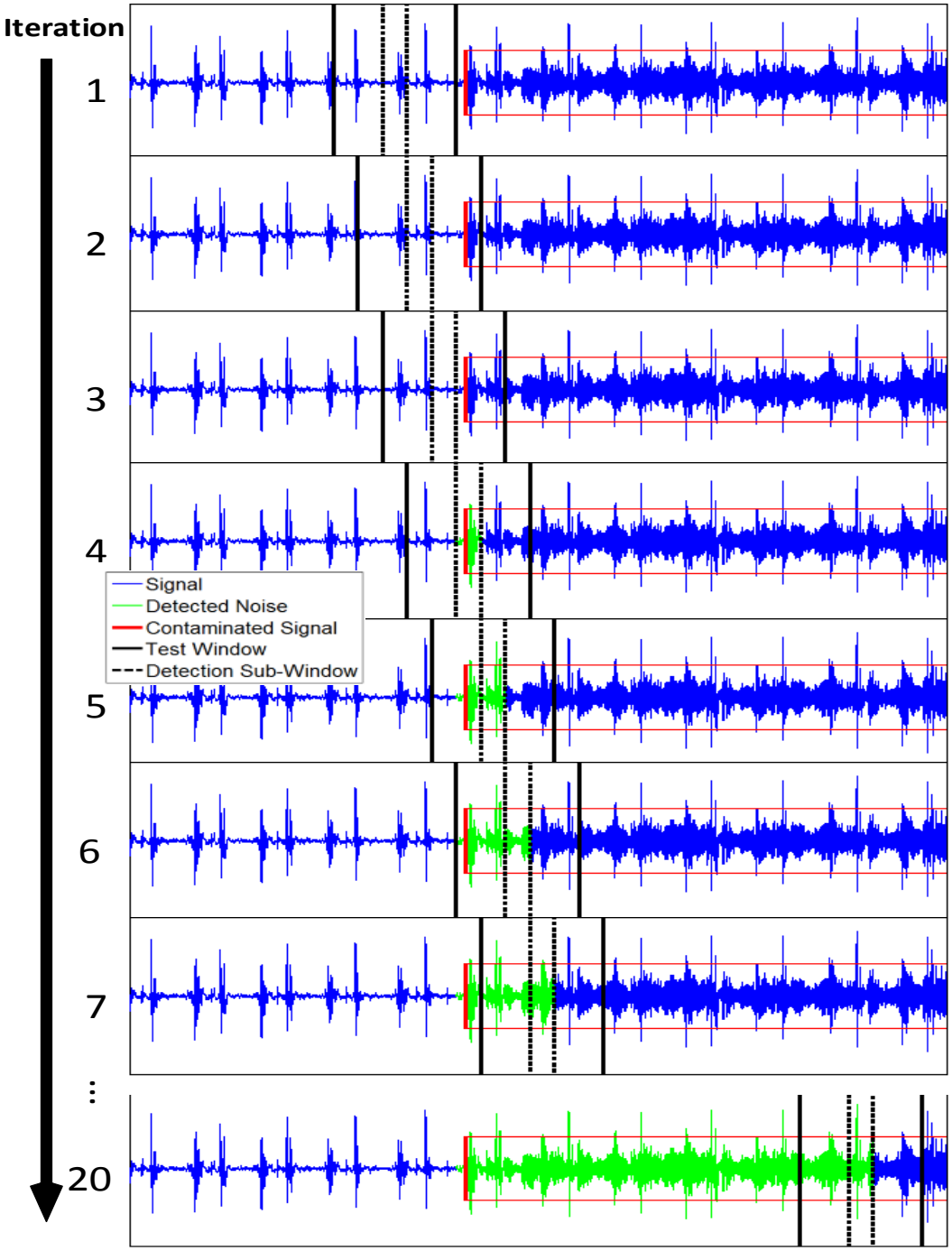
Iteration
1
2
3
4
5
6
7
⋮
20
Signal
Detected Noise
Contaminated Signal
Test Window
Detection Sub-Window

Appendix B

In the following tables are presented the false positive rate on the different heartbeat and rhythms types, for each lead.

- MLII

Beat Type	Detected Percentage (%)	Total Number
Normal	6,64	24551
Left bundle branch block beat	8,27	1207
Right bundle branch block beat	3,79	1125
APC	7,71	819
Aberrated APC	19,78	23
Nodal premature beat	26,04	12
PVC	9,14	1801
Fusion of ventricular and normal beat	11,91	220
Nodal escape beat	6,94	3
Ventricular escape beat	0,00	1
Paced beat	4,46	1196
Non-conducted P-wave (blocked APC)	11,57	71

Rhythm Type	Detected Percentage (%)	Total Time (s)
Atrial fibrillation	5,91	4614
Ventricular bigeminy	12,53	299
Normal sinus rhythm	6,68	27664
Nodal rhythm	28,03	13
Paced rhythm	4,68	1494
Pre-excitation	8,25	575
Sinus bradycardia	5,25	1400
Supraventricular tachyarrhythmia	78,87	14
Ventricular trigeminy	7,82	457
Ventricular tachycardia	41,86	5

- V1

Beat Type	Detected Percentage (%)	Total Number
Normal	7,05	18917
Left bundle branch block beat	5,66	3430
Right bundle branch block beat	7,77	1887
APC	4,50	364
Aberrated APC	8,58	68
Nodal premature beat	0,00	1
PVC	10,16	1936
Fusion of ventricular and normal beat	24,81	249
Atrial escape beat	3,89	10
Nodal escape beat	8,47	99
Ventricular escape beat	0,63	105
Paced beat	7,69	2202
Fusion of paced and normal beat	8,37	150
Ventricular flutter wave	19,03	193
Non-conducted P-wave (blocked APC)	7,57	94

Rhythm Type	Detected Percentage (%)	Total Time (s)
Atrial bigeminy	1,92	117
Atrial fibrillation	3,43	2816
Atrial flutter	3,70	420
Ventricular bigeminy	11,01	1133
2° heart block	23,94	520
Idioventricular rhythm	1,09	157
Normal sinus rhythm	7,24	22619
Nodal rhythm	7,67	158
Paced rhythm	7,76	2921
Pre-excitation	6,28	604
Supraventricular tachyarrhythmia	1,26	85
Ventricular trigeminy	3,46	408
Ventricular flutter	18,06	93
Ventricular tachycardia	16,36	50

- V2

Beat Type	Detected Percentage (%)	Total Number
Normal	4,25	2049
PVC	6,94	4
Paced beat	6,04	1951
Fusion of paced and normal beat	13,75	432
Unclassifiable beat	0,00	3

Rhythm Type	Detected Percentage (%)	Total Time (s)
Normal sinus rhythm	5,12	2983
Paced rhythm	6,50	2778

- V5

Beat Type	Detected Percentage (%)	Total Number
Normal	3,77	3523
APC	3,47	24
Nodal premature beat	0,00	2
PVC	7,30	35
Fusion of ventricular and normal beat	0,00	2
Paced beat	5,79	1961
Fusion of paced and normal beat	19,22	427
Unclassifiable beat	0,00	3

Rhythm Type	Detected Percentage (%)	Total Time (s)
Normal sinus rhythm	4,64	4929
Paced rhythm	6,44	2780
Supraventricular tachyarrhythmia	0,00	7